The $Te(OTeF_5)_5^-$ and $FTe(OTeF_5)_4^-$ Anions: Synthesis, X-ray Structure Determinations, and Raman Spectra of $Te(OTeF_5)_4$ and $N(CH_3)_4^+Te(OTeF_5)_5^-$ and Solution Characterization of the $FTe(OTeF_5)_4^-$ and $Te(OTeF_5)_5^-$ Anions by ^{19}F and ^{125}Te NMR Spectroscopy

Hélène P. A. Mercier, Jeremy C. P. Sanders, and Gary J. Schrobilgen*

Department of Chemistry, McMaster University, Hamilton, Ontario L8S 4M1, Canada

Received March 10, 1994[⊗]

The Lewis acid behavior of $Te(OTeF_5)_4$ toward the $OTeF_5^-$ anion has been investigated, and the resulting $Te(OTeF_5)_5^-$ and $FTe(OTeF_5)_4^-$ anions have been structurally characterized in solution as the tetramethylammonium and tetraethylammonium salts by ^{19}F and ^{125}Te NMR spectroscopy. The crystal structures and Raman spectra are reported for $Te(OTeF_5)_4$ and $N(CH_3)_4^+Te(OTeF_5)_5^-$. The former compound crystallizes in the triclinic system, space group $P\bar{1}$, with $a = 9.502(3)$ Å, $b = 9.748(5)$ Å, $c = 10.603(4)$ Å, $\alpha = 85.73(4)°$, $\beta = 72.50(3)°$, and $\gamma = 71.26(3)°$ at −97 °C; V = 886.7(6) Å^3; $D_{calc} = 4.052$ g cm^{-3} for $Z = 2$; $R_1 = 0.0239$. The salt, $N(CH_3)_4^+Te(OTeF_5)_5^-$, crystallizes in the orthorhombic system, space group *Pbca*, with $a = 11.021(2)$ Å, $b = 20.096(5)$ Å, $c = 27.497(5)$ Å at 24 °C; V = 6090(2) Å^3; $D_{calc} = 3.042$ g cm^{-3} for $Z = 8$; w$R = 0.0781$. The $Te(OTeF_5)_4$ molecule is a disphenoid and is consistent with an AX_4E VSEPR geometry in which a lone electron pair and two $OTeF_5$ groups occupy the equatorial plane and two $OTeF_5$ groups occupy the axial positions of a trigonal bipyramid. Two secondary $Te^{IV}\cdots F$ contacts arising from two nearest neighbor $Te(OTeF_5)_4$ molecules give rise to a chain structure in which the coordination about Te^{IV} is best described as a distorted octahedral (AX_4Y_2E) VSEPR arrangement. The central Te^{IV} atom of the $Te(OTeF_5)_5^-$ anion is bonded to five $OTeF_5$ groups, so that the gross geometry about the Te^{IV} atom can be described as pseudo-octahedral. The presence of a bulky $OTeF_5$ group in the axial position influences the conformational relationships of the equatorial $OTeF_5$ groups. Solution NMR studies establish that the $FTe(OTeF_5)_4^-$ anion is pseudo-octahedral about the Te^{IV} atom and that the fluorine bonded to Te^{IV} is in the axial position opposite the lone electron pair. The coordination in the Te^{IV} valence shells of the $Te(OTeF_5)_5^-$ and $FTe(OTeF_5)_4^-$ anions is consistent with an AX_5E VSEPR arrangement of five bond pairs and a lone electron pair. The $Te(OTeF_5)_5^-$ and TeF_5^- anions were shown to undergo ligand redistribution and, with the exception of $FTe(OTeF_5)_4^-$, the intermediate $F_nTe(OTeF_5)_{5-n}^-$ anions were found to be labile on the NMR time scale.

Introduction

The Lewis acidities of $OTeF_5$-substituted complexes of the main-group elements have been little studied. We have previously prepared $As(OTeF_5)_5$ and $Bi(OTeF_5)_5$ and shown that they function as strong $OTeF_5^-$ anion acceptors forming the $As(OTeF_5)_6^-$ [1,2] and $Bi(OTeF_5)_6^-$ [3] anions. Although the precursor to the $Sb(OTeF_5)_6^-$ anion, $Sb(OTeF_5)_5$, is unstable, this anion has also been synthesized by a different route and characterized in the solid state.[3] Substitution of $OTeF_5$ groups for fluorines in the BF_4^- and MF_6^- anions (M = As, Sb, Bi) is expected to result in a dramatic lowering of the basicities of the resulting anions by dispersing the negative charge over 20 and 30 rather than 4 and 6 fluorines, respectively. Consequently, $As(OTeF_5)_6^-$, $Sb(OTeF_5)_6^-$, and $Bi(OTeF_5)_6^-$ and the fully $OTeF_5$-substituted transition metal anions, $Nb(OTeF_5)_6^-$,[4,5] $Ta(OTeF_5)_6^-$,[4] $Pd(OTeF_5)_4^{2-}$,[6] and $Ti(OTeF_5)_6^{2-}$,[7] offer promise as very weakly coordinating anions. References 3, 8, and 9 should be consulted for overviews of the subject.

The present study extends this work to a coordinately unsaturated $OTeF_5$ derivative of a main-group VI element, namely, $Te(OTeF_5)_4$. The structure and $OTeF_5$ donor properties of $Te(OTeF_5)_4$ and the mixed derivatives, $F_xTe(OTeF_5)_{4-x}$, toward $As(OTeF_5)_5$ have been previously established in solution by ^{19}F and ^{125}Te NMR spectroscopy.[2] Unlike TeF_4, which is extensively fluorine bridged in the solid state[10] and undergoes intermolecular fluorine exchange in solution by means of fluorine-bridged intermediates,[11] the $OTeF_5$ groups of $Te(OTeF_5)_4$ were shown to be nonlabile with respect to intermolecular exchange in solution.[2,12] The difference in exchange behavior between TeF_4 and $Te(OTeF_5)_4$ is attributed to the greater steric crowding in $Te(OTeF_5)_4$, rendering the formation of bridged intermediates more difficult. The $Te(OTeF_5)_4$ molecule was, however, shown to be fluxional on the NMR time scale.[2,12] The exchange is consistent with the axial and

[⊗] Abstract published in *Advance ACS Abstracts,* September 15, 1995.

(1) Collins, M. J.; Rao, U. R. K.; Schrobilgen, G. J. *J. Magn. Reson.* **1985**, *61*, 137.
(2) Collins, M. J.; Schrobilgen, G. J. *Inorg. Chem.* **1985**, *24*, 2608.
(3) Mercier, H. P. A.; Sanders, J. C. P.; Schrobilgen, G. J. *J. Am. Chem. Soc.* **1994**, *116*, 2921.
(4) Moock, K.; Seppelt, K. *Z. Anorg. Allg. Chem.* **1988**, *561*, 132.
(5) Rack, J. J.; Moasser, B.; Gargulak, J. D.; Gladfelter, W. L.; Hochheimer, H. D.; Strauss, S. H. *J. Chem. Soc., Chem. Comm.* **1994**, 685.
(6) Colsman, M. R.; Newbound, T. D.; Marshall, L. J.; Noirot, M. D.; Miller, M. M.; Wulfsberg, G. P.; Frye, J. S.; Anderson, O. P.; Strauss, S. H. *J. Am. Chem. Soc.* **1990**, *112*, 2349.
(7) Schröder, K.; Sladky, F. *Chem. Ber.* **1980**, *113*, 1414.
(8) Strauss, S. H. *Chem. Rev.* **1993**, *93*, 927.
(9) Hurlburt, P. K.; Van Seggen, D. M.; Rack, J. J.; Strauss, S. H. *Inorganic Fluorine Chemistry Toward the 21st Century*; Thrasher, J. S., Strauss, S. H., Eds.; American Chemical Society: Washington, DC, 1994; pp 338–349.
(10) Edwards, A. J.; Hewaidy, F. I. *J. Chem. Soc. A* **1968**, 2977.
(11) Muetterties, E. L.; Phillips, W. D. *J. Am. Chem. Soc.* **1959**, *81*, 1084.
(12) Birchall, T.; Myers, R. D.; de Waard, H.; Schrobilgen, G. J. *Inorg. Chem.* **1982**, *21*, 1068.

0020-1669/95/1334-5261$09.00/0

equatorial $OTeF_5$ groups of the AX_4E molecule undergoing rapid intramolecular exchange by means of a Berry pseudorotation. The crystal structure of the related $F_2Te(OTeF_5)_2$ molecule has been determined in $O{=}Re(OTeF_5)_4{\cdot}F_2Te(OTeF_5)_2$,[13] but no detailed structure determination of $Te(OTeF_5)_4$ has been reported.

Although the fluoride acceptor properties of TeF_4 and the existence of the TeF_5^- anion are well documented both in solution,[14-17] and in the solid state,[14,16,18] the $OTeF_5^-$ acceptor properties of $Te(OTeF_5)_4$ and the formation of the $Te(OTeF_5)_5^-$ anion had not been demonstrated prior to the present study. The X-ray crystal structures of several related ionic and neutral square-planar and pseudo-octahedral main-group and square pyramidal transition metal $OTeF_5$ derivatives have been previously determined, namely, $O{=}I(OTeF_5)_4^-$,[19] $I(OTeF_5)_4^-$,[19] $Xe(OTeF_5)_4$,[20] $O{=}Mo(OTeF_5)_4$,[21,22] $O{=}W(OTeF_5)_4$,[22] $O{=}Re(OTeF_5)_4$,[13] and $O{=}Os(OTeF_5)_4$.[21] The iodine(V) derivatives $FI(OTeF_5)_4$[23] and $I(OTeF_5)_5$[23] have been synthesized and are isoelectronic with the $FTe(OTeF_5)_4^-$ and $Te(OTeF_5)_5^-$ anions, but their X-ray crystal structures have not been determined. In the aforementioned cases, where crystal structures have been determined, the axial positions are occupied by a doubly bonded oxygen or a lone electron pair, whereas the $Te(OTeF_5)_5^-$ anion affords the opportunity to study the steric effects of a bulky $OTeF_5$ group in the axial position of a pseudo-octahedron.

The present work reports the crystal structure of the $Te(OTeF_5)_4$ molecule, as well as the synthesis of the $Te(OTeF_5)_5^-$ anion as its $N(CH_3)_4^+$ salt and its characterization in solution by ^{19}F and ^{125}Te NMR spectroscopy and in the solid state by X-ray crystallography and Raman spectroscopy. The structurally related $FTe(OTeF_5)_4^-$ anion has also been characterized in solution by ^{19}F and ^{125}Te NMR spectroscopy.

Results and Discussion

Syntheses of the $Te(OTeF_5)_5^-$ and $FTe(OTeF_5)_4^-$ Anions. Although the Lewis acidity of $Te(OTeF_5)_4$ is expected to be less than that of TeF_4, the synthesis of the hitherto unknown $Te(OTeF_5)_5^-$ anion has been achieved using a synthetic route analogous to that used for the preparation of $As(OTeF_5)_6^-$ as the $N(CH_3)_4^+$ salt[3] (eq 1). The reaction proceeds at ambient

$$Te(OTeF_5)_4 + N(CH_3)_4{}^+OTeF_5{}^- \xrightarrow[25\ °C]{SO_2ClF} N(CH_3)_4{}^+Te(OTeF_5)_5{}^- \quad (1)$$

temperature to yield a colorless solution in the weakly coordinating solvent, SO_2ClF. The salt, $N(CH_3)_4{}^+Te(OTeF_5)_5{}^-$, was isolated as a colorless, stable, crystalline solid by allowing Freon 114, in which the salt is insoluble, to diffuse slowly into the SO_2ClF solutions.

All $N(CH_3)_4{}^+Te(OTeF_5)_5{}^-$ preparations were contaminated with small amounts of $N(CH_3)_4{}^+FTe(OTeF_5)_4{}^-$ (ca. 5−10%) which are believed to arise from incomplete conversion of TeF_4 with excess $B(OTeF_5)_3$ in the preparation of the starting material, $Te(OTeF_5)_4$.[12,24] Moreover, the $FTe(OTeF_5)_4^-$ salt is even less soluble in the Freon 114/SO_2ClF mixtures used for recrystallization and, therefore, was concentrated in the recrystallized product, resulting in the adventitious characterization of the $FTe(OTeF_5)_4^-$ anion in SO_2ClF solution by NMR spectroscopy (see **NMR Spectroscopy of $Te(OTeF_5)_5^-$ and $FTe(OTeF_5)_4^-$**).

Higher concentrations of the $FTe(OTeF_5)_4^-$ anion in SO_2ClF solution were generated by the interaction of XeF_2 with $N(CH_3)_4{}^+Te(OTeF_5)_5{}^-$ at −50 °C according to eq 2.

$$2Te(OTeF_5)_5{}^- + XeF_2 \xrightarrow[-50\ °C]{SO_2ClF} 2FTe(OTeF_5)_4{}^- + Xe(OTeF_5)_2 \quad (2)$$

Warming of the solution to room temperature resulted in F/$OTeF_5$ scrambling and the formation of the mixed-anion series $F_nTe(OTeF_5)_{5-n}^-$ according to eq 3. Although the neutral

$$FTe(OTeF_5)_4{}^- + nXeF_2 \xrightarrow[25\ °C]{SO_2ClF} F_nTe(OTeF_5)_{5-n}{}^- + nFXeOTeF_5 \quad (3)$$

isoelectronic iodine analog, $FI(OTeF_5)_4$, undergoes thermal decomposition at 80 °C according to eq 4,[23] the analogous decomposition of the $FTe(OTeF_5)_4^-$ anion was not apparent under the conditions employed to prepare and study this anion.

$$FI(OTeF_5)_4 \rightarrow O{=}I(OTeF_5)_3 + TeF_6 \quad (4)$$

Ligand redistribution has been established when $I(OTeF_5)_5$ dissolves in IF_5 to give the entire series of mixed $F_nI(OTeF_5)_{5-n}$ species.[23] Mixtures of $N(n\text{-}Bu)_4{}^+TeF_5{}^-$ and either $N(CH_2CH_3)_4{}^+Te(OTeF_5)_5{}^-$ or $N(CH_3)_4{}^+Te(OTeF_5)_5{}^-$ undergo ligand redistribution in CH_2Cl_2 and SO_2ClF solvents, respectively, upon dissolution at ambient temperatures. However, other than $FTe(OTeF_5)_4^-$, chemical exchange and extensive spectral overlap precluded identification and NMR spectral assignments of individual $F_nTe(OTeF_5)_{5-n}^-$ ($n = 2-4$) anions and their isomers.

NMR Spectroscopy of $Te(OTeF_5)_5^-$ and $FTe(OTeF_5)_4^-$ Anions. The ^{19}F and ^{125}Te NMR spectra of $N(CH_3)_4{}^+Te(OTeF_5)_5{}^-$ in SO_2ClF are shown in Figures 1 and 2, and their NMR parameters are listed in Table 1. The ^{125}Te NMR spectrum appears as two overlapping sets of doublets of quintets in the fluorine-on-tellurium(VI) region of the spectrum arising from the coupling of ^{125}Te to the ^{19}F ligands of the four equatorial $OTeF_5$ groups and the single axial $OTeF_5$ group. The ^{125}Te multiplets clearly have an asymmetric appearance which is attributed to higher-order effects. Such effects have been noted previously for other $OTeF_5$ derivatives and arise from the very small difference in chemical shift between the F_A and F_B environments and relatively large sizes of $^1J(^{125}Te-^{19}F_A)$ and $^1J(^{125}Te-^{19}F_B)$.[3,12,25] The $^{125}Te^{VI}$ spectrum of the minor impurity attributable to the $FTe(OTeF_5)_4^-$ anion is observed to low frequency of $Te(OTeF_5)_5^-$. The $^{125}Te^{IV}$ chemical shifts of $Te(OTeF_5)_5^-$ (1122.9 ppm) and $FTe(OTeF_5)_4^-$ (1083.6 ppm) are similar to that previously reported for TeF_5^-,[17] which occurs at 1142.2 ppm in CH_2Cl_2 at −39 °C in the present study (Table 1 and Supporting Information Figure 7). The ^{125}Te NMR

(13) Turowsky, L.; Seppelt, K. *Z. Anorg. Allg. Chem.* **1990**, *590*, 37.
(14) Morris, R. J.; Moss, K. C. *J. Fluorine Chem.* **1979**, *13*, 551.
(15) Gorrell, I. B.; Ludman, C. J.; Matthews, R. S. *J. Chem. Soc., Dalton Trans.* **1992**, 2899.
(16) Mahjoub, A. R.; Leopold, D.; Seppelt, K. *Z. Anorg. Allg. Chem.* **1990**, *590*, 23.
(17) Kokunov, Y. V.; Gorbunova, Y. E.; Afamasjev, V. M.; Petrov, V. N.; Davidovich, R. L.; Buslav, Y. A. *J. Fluorine Chem.* **1990**, *50*, 285.
(18) Martin, S. H.; Ryan, R. R.; Asprey, L. B. *Inorg. Chem.* **1970**, *9*, 2100.
(19) Turowsky, L.; Seppelt, K. *Z. Anorg. Allg. Chem.* **1991**, *602*, 79.
(20) Turowsky, L.; Seppelt, K. *Z. Anorg. Allg. Chem.* **1992**, *609*, 153.
(21) Von Huppmann, P.; Labischinski, H.; Lentz, D.; Pritzkow, H.; Seppelt, K. *Z. Anorg. Allg. Chem.* **1982**, *487*, 7.
(22) Turowsky, L.; Seppelt, K. *Z. Anorg. Allg. Chem.* **1990**, *590*, 23.
(23) Lentz, D.; Seppelt, K. *Angew. Chem., Int. Ed. Engl.* **1978**, *17*, 355.
(24) Lentz, D.; Pritzkow, H.; Seppelt, K. *Inorg. Chem.* **1978**, *17*, 1926.
(25) Damerius, R.; Huppmann, P.; Lentz, D.; Seppelt, K. *J. Chem. Soc., Dalton Trans.* **1984**, 2821.

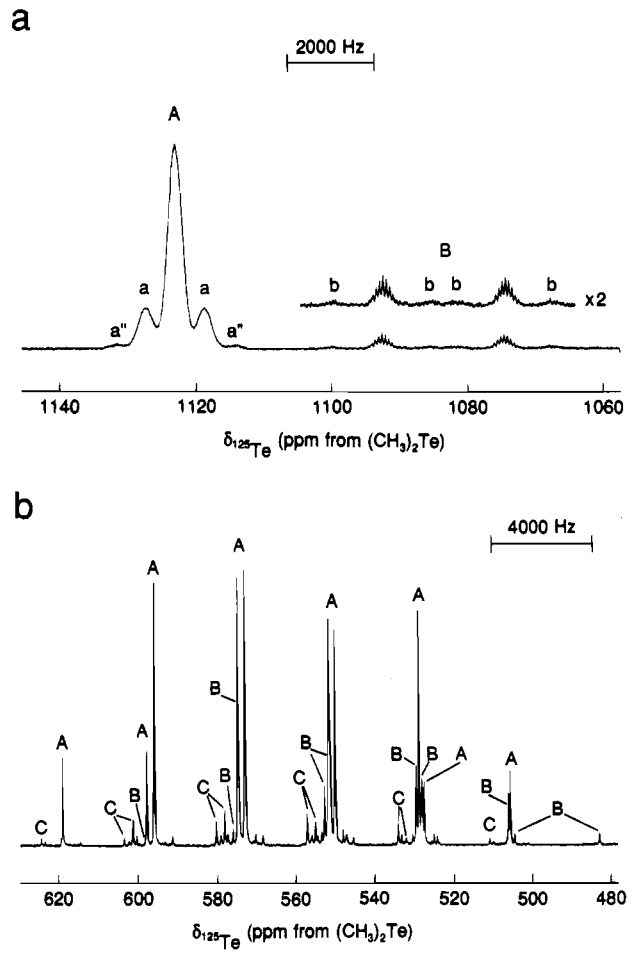

Figure 1. ^{125}Te NMR spectrum (157.794 MHz) of $N(CH_3)_4^+Te(OTeF_5)_5^-$ in SO_2ClF at −50 °C. (a) Te(IV) region: (A) $Te(OTeF_5)_5^-$; (B) $FTe(OTeF_5)_4^-$. The lower case lables (a, a″, and b) refer to $^{125}Te(VI)$ satellites arising from the $Te(O^{125}TeF_5)(OTeF_5)_4^-$, $Te(O^{125}TeF_5)_2(OTeF_5)_3^-$, and $FTe(O^{125}TeF_5)(OTeF_5)_3^-$ isotopomers, respectively. (b) Te(VI) region: (A) $(OTeF_5)_{eq}$ of $Te(OTeF_5)_5^-$; (B) $(OTeF_5)_{ax}$ of $Te(OTeF_5)_5^-$; (C) $(OTeF_5)_{eq}$ of $FTe(OTeF_5)_4^-$. The low-intensity peaks at the bases of the main resonances are ^{125}Te satellites arising from the two-bond coupling of $^{125}Te(VI)$ to $^{125}Te(IV)$.

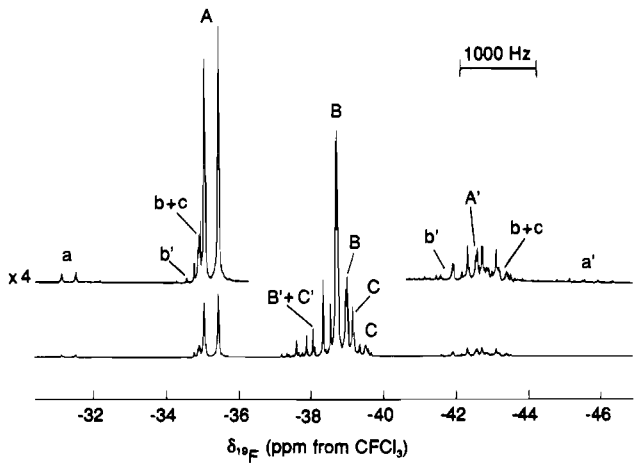

Figure 2. ^{19}F NMR spectrum (470.599 MHz) of $N(CH_3)_4^+Te(OTeF_5)_5^-$ in SO_2ClF at −50 °C: (A) $F(B_4)$ of $(OTeF_5)_{ax}$ of $Te(OTeF_5)_5^-$; (A′) F(A) of $(OTeF_5)_{ax}$ of $Te(OTeF_5)_5^-$; (B) $F(B_4)$ of $(OTeF_5)_{eq}$ of $Te(OTeF_5)_5^-$; (B′) F(A) of $(OTeF_5)_{eq}$ of $Te(OTeF_5)_5^-$; (C) $F(B_4)$ of $(OTeF_5)_{eq}$ of $FTe(OTeF_5)_4^-$; (C′) F(A) of $(OTeF_5)_{eq}$ of $FTe(OTeF_5)_4^-$. Lower case letters denote ^{125}Te satellites.

spectrum of $Te(OTeF_5)_5^-$ in the Te^{IV} region consists of a broad line with two sets of ^{125}Te satellites arising from overlapping $^2J(^{125}Te^{IV}-^{125}Te^{VI})$ couplings with the axial and equatorial $OTeF_5$ groups in the most abundant isotopomers $Te(O^{125}TeF_5)(OTeF_5)_4^-$ and $Te(O^{125}TeF_5)_2(OTeF_5)_3^-$. The Te^{IV} resonance of $FTe(OTeF_5)_4^-$ also exhibits a doublet splitting arising from $^1J(^{19}F_A-^{125}Te^{IV})$ which is very similar to the corresponding coupling in the TeF_5^- anion (Table 1). Each doublet branch is further split into an odd-line multiplet that arises from the three-bond coupling, $^3J(^{19}F_{eq}-^{125}Te^{IV})$. The central Te^{IV} and the equatorial fluorines of the $OTeF_5$ groups are expected to exhibit this three-bond coupling because the corresponding $^3J(^{19}F_{eq}-^{129}Xe)$ couplings in $F_xXe(OTeF_5)_{4-x}$ and $O{=}XeF_x(OTeF_5)_{4-x}$ ($x = 0-4$)[26,27] are well resolved even though ^{129}Xe has a smaller gyromagnetic ratio than ^{125}Te. This coupling is also well resolved in the case of the $FTe(OTeF_5)_4^-$ anion where there is only a single equatorial $OTeF_5$ environment but is not observed for the $Te(OTeF_5)_5^-$ anion. The $^{125}Te^{IV}$ resonance of $Te(OTeF_5)_5^-$ is, however, broad and this broadening is presumed to arise from overlap of two coupling patterns arising from the equatorial fluorines of both the axial and equatorial $OTeF_5$ groups to give an unresolved septodecet of quintets. In both axial and equatorial $OTeF_5$ groups, the couplings of the axial fluorines of the $OTeF_5$ groups are expected to be small (cf. 4 Hz in $O{=}Xe(OTeF_5)_4$[27]) and are not resolved.

The ^{19}F NMR spectrum of the $Te(OTeF_5)_5^-$ anion consists of two overlapping AB_4 patterns in the ratio 4:1 corresponding to the equatorial and axial environments of the $OTeF_5$ groups (Table 1 and Figure 2). The AB_4 patterns are characteristic of $OTeF_5$ derivatives with chemical shifts and $^2J(^{19}F_A-^{19}F_B)$ values for these resonances falling within the normal range found for other $OTeF_5$ derivatives.[3,12,28,29] The frequency separations between $\delta(F_A)$ and $\delta(F_B)$ for the axial and equatorial environments are sufficiently large to give well resolved AB_4 patterns which could be analyzed and computer-simulated in order to extract the values of $^2J(^{19}F_A-^{19}F_B)$. The spectra also display ^{125}Te and ^{123}Te satellites flanking the main resonances. These satellites have an asymmetric appearance arising from second order effects associated with the coupling of the AB_4 spin systems to $^{123,125}Te$ as discussed in the section on the ^{125}Te NMR spectra (*vide supra*). In addition, the spectrum also reveals a weak AB_4 pattern and a singlet with ^{125}Te satellites which are attributable to the $FTe(OTeF_5)_4^-$ impurity (Table 1 and Figure 2). Both ^{19}F and ^{125}Te spectra are consistent with the fluorine being bonded to Te^{IV} in the axial position trans to the lone electron pair. The chemical shift of the axial fluorine (−15.2 ppm) is more shielded than that of TeF_5^- ($N(n\text{-}Bu)_4^+TeF_5^-$: −30.1 ppm, −39 °C in CH_2Cl_2 solvent).

The $FTe(OTeF_5)_4^-$ anion was obtained in high concentrations in SO_2ClF solution according to ligand exchange reaction 3 and did not form the $F_2Te(OTeF_5)_5^-$ anion as hoped for. The ^{19}F NMR spectra of the products of the reaction between $N(CH_2CH_3)_4^+Te(OTeF_5)_5^-$ and a 50 mol % excess of XeF_2 in SO_2ClF solvent were recorded after warming the sample from −196 to −50 °C; no gas evolution was noted upon warming. The ^{19}F NMR spectrum of the reaction products exhibited two new singlets and two new AB_4 spin patterns. The two AB_4 spin patterns attributed to the $Te(OTeF_5)_5^-$ anion were no longer present. An intense singlet at −15.3 ppm, along with its ^{125}Te satellites ($^1J(^{125}Te-^{19}F)$, 2874 Hz), was assigned to the F-on-Te^{IV} environment of $FTe(OTeF_5)_4^-$ and corresponded to the impurity in the ^{19}F NMR spectrum of $Te(OTeF_5)_5^-$ (*vide supra*). A weaker singlet at −176.8 ppm, with ^{129}Xe satellites ($^1J(^{129}Xe-^{19}F)$, 5607 Hz), was assigned to unreacted XeF_2. The more

(26) Schumacher, G. A.; Schrobilgen, G. J. *Inorg. Chem.* **1984**, *23*, 2923.
(27) Jacob, E.; Lentz, D.; Seppelt, K.; Simon, A. *Z. Anorg. Allg. Chem.* **1981**, *472*, 7.
(28) Seppelt, K. *Z. Anorg. Allg. Chem.* **1973**, *399*, 65.
(29) Schrobilgen, G. J.; Keller, N. *Inorg. Chem.* **1981**, *20*, 2118.

Table 1. ^{19}F and ^{125}Te NMR Data for $Te(OTeF_5)_5^-$, $FTe(OTeF_5)_4^-$, and TeF_5^-

	chem shifts, ppm[a]				coupling constants, Hz[a]			
	$\delta(^{19}F)_A$	$\delta(^{19}F)_B$	$\delta(^{125}Te^{VI})$	$\delta(^{125}Te^{IV})$	$^2J(^{19}F_A-^{19}F_B)$	$^1J(^{19}F_A-^{125}Te)$	$^1J(^{19}F_B-^{125}Te)$	$^2J(^{125}Te^{VI}-^{125}Te^{IV})$
$Te(OTeF_5)_5^-$ [b,c]								
$(OTeF_5)_{ax}$	−42.5	−35.2	540.2	1122.9[d]	186	3431	3677	1414
$(OTeF_5)_{eq}$	−38.1	−38.8	562.4		183	3334	3641	1207
$FTe(OTeF_5)_4^-$ [d,e]								
$(OTeF_5)_{eq}$	−37.8 (−36.7)	−39.3 (−40.2)	567.5	1083.6	(177)[f]	3308	3651	2116
F_A	−15.2 (−17.3)					2844 (2880)		
TeF_5^- [g]								
	−30.1	−39.5		1142.2	50.9	2890	1379	

[a] The axial and equatorial environments of the $OTeF_5$ groups and of the TeF_5^- anion are designated by A and B, respectively. [b] Spectra were recorded in SO_2ClF solvent at −50 °C for the $N(CH_3)_4^+$ salts. [c] The $^3J(^{125}Te^{IV}-^{19}F_A)$ couplings are too small to be resolved (cf. ref 22). [d] The central line and its satellites are broad owing to unresolved splittings arising from the $^3J(^{125}Te^{IV}-^{19}F_B)$ coupling constants of the axial and equatorial $OTeF_5$ groups. [e] $^1J(^{125}Te^{IV}-^{19}F_A)$, 2844 Hz; $^3J(^{125}Te^{IV}-^{19}F_B)$, 76 Hz. [f] Values in parentheses are from spectra recorded at for a 1:1 molar mixture of $N(CH_3)_4^+Te(OTeF_5)_5^-/N(n\text{-}Bu)_4^+TeF_5^-$ in SO_2ClF solvent at −60 °C. [g] Spectrum recorded in CH_2Cl_2 at −39 °C. The ^{19}F NMR parameters differ significantly from those reported in ref 13. The reported values of $^2J(^{19}F_A-^{19}F_B) = 105$ Hz, $\delta(^{19}F_A) = -28.4$ ppm, and $\delta(^{19}F_B) = -42$ ppm are also in marked variance to the values reported in refs 11 and 12, which also use CH_2Cl_2 as the solvent. The differences may arise because a coordinating solvent, CH_3CN, was used in the former study and may strongly coordinate to Te(IV). Acetonitrile is apparently a relatively strong electron-pair donor toward $Te(OTeF_5)_4$.[10]

intense of the two AB_4 spin patterns corresponded to the equatorial $OTeF_5$ ligands of $FTe(OTeF_5)_4^-$, while the less intense AB_4 spin pattern was assigned to $Xe(OTeF_5)_2$. When the sample was warmed to 25 °C and the spectrum was recorded at −50 °C, the singlet and AB_4 spin patterns attributed to $FTe(OTeF_5)_4^-$ disappeared, while the resonance attributed to $Xe(OTeF_5)_2$ increased significantly in intensity. Only the B part of the AB_4 spectrum of $FXeOTeF_5$ ($\delta(^{19}F_B) = -46.3$ ppm, $^1J(^{125}Te-^{19}F_B) = 3621$ Hz, $^2J(^{19}F_A-^{19}F_B) = 179$ Hz) was observed because the A multiplet severely overlapped with the AB_4 patterns of the mixed-anion series, $F_nTe(OTeF_5)_{5-n}^-$ ($n = 2-5$), but is in good agreement with the published data.[28] The F-on-Xe^{II} environment of $FXeOTeF_5$, a singlet with ^{129}Xe satellites, was located at −151.0 ppm; $^1J(^{129}Xe-^{19}F)$, 5729 Hz. Warming to 25 °C resulted in further ligand exchange, consuming all of the $FTe(OTeF_5)_4^-$ anion present and producing the series of mixed F/$OTeF_5$ substituted Te^{IV} anions, $F_nTe(OTeF_5)_{5-n}^-$ ($n = 2-5$) according to eq 3. These anions gave a complex series of overlapping AB_4 patterns in the range of −33 to −43 ppm and could not be assigned. Failure to observe F-on-Te^{IV} environments other than that of $FTe(OTeF_5)_4^-$ is attributed to intermediate fluorine exchange among F-on-Te^{IV} environments which presumably occurs through Te^{IV}- - -F- - -Te^{IV} bridge formation (*vide infra*).

Ligand redistribution reactions have also been investigated for the mixtures $N(CH_3)_4^+Te(OTeF_5)_5^-/N(n\text{-}Bu)_4^+TeF_5^-$ in SO_2ClF solvent and $N(CH_2CH_3)_4^+Te(OTeF_5)_5^-/N(n\text{-}Bu)_4^+TeF_5^-$ in CH_2Cl_2. The ^{19}F NMR spectrum of a 1:2 molar mixture in SO_2ClF solvent at −60 °C shows a well-resolved AX_4 pattern (superimposed on a broad resonance centered at ca. −36.5 ppm ($\Delta\nu_{1/2} \sim 2000$ Hz). The AX_4 pattern ($\delta(^{19}F_A) = -32.7$ ppm, $\delta(^{19}F_X) = -40.5$ ppm, $^2J(^{19}F_A-^{19}F_X) = 181.3$ Hz, $^1J(^{125}Te-^{19}F_A) = 3135$ Hz, $^1J(^{125}Te-^{19}F_X) = 3658$ Hz) was assigned to $OTeF_5$ groups undergoing rapid intermolecular exchange, while the F-on-Te^{IV} environments again were not observed owing to intermediate intermolecular fluorine exchange and are assigned to the broad resonance at −36.5 ppm. At a 1:1 molar ratio in SO_2ClF solvent, the axial fluorine of $FTe(OTeF_5)_4^-$ was observed at −17.3 ppm as a broadened line with ^{125}Te satellites ($^1J(^{125}Te-^{19}F_A) = 2880$ Hz) and the broadened AB_4 pattern of the $FTe(OTeF_5)_4^-$ anion ($\delta(^{19}F_A) = -36.7$ ppm, $\delta(^{19}F_B) = -40.2$ ppm, $^2J(^{19}F_A-^{19}F_B) = 177$ Hz) was also observed along with an intense AX_4 spectrum assigned to rapidly exchanging $OTeF_5$ groups of the higher fluorinated anions ($\delta(^{19}F_A) = -33.5$ ppm, $\delta(^{19}F_X) = -40.6$ ppm, $^2J(^{19}F_A-^{19}F_X) = 179$ Hz). Failure to observe F-on-Te^{IV} environments for other than the $FTe(OTeF_5)_4^-$ anion is attributed to intermediate intermolecular fluorine exchange which results in a broad fluorine resonance that is indistinguishable from the spectral baseline. The ^{125}Te NMR spectrum of a 1:1 molar ratio of $Te(OTeF_5)_5^-/TeF_5^-$ in CH_2Cl_2 at −50 °C consisted of a series of broad overlapping multiplets in the Te^{IV} region (1165−1180 ppm), while the Te^{VI} region showed a sharp doublet of quintets ($\delta(^{125}Te) = 570.3$ ppm, $^1J(^{125}Te-^{19}F_{ax}) = 3283$ Hz, $^1J(^{125}Te-^{19}F_{eq}) = 3679$ Hz) overlapped by an intense broad doublet of quintets ($\delta(^{125}Te) = 574$ ppm, $^1J(^{125}Te-^{19}F_{ax}) = 3038$ Hz, $^1J(^{125}Te-^{19}F_{eq}) = 3638$ Hz). Although the broadened multiplets in the Te^{IV} region of the spectrum arise from $^{19}F-^{125}Te^{IV}$ coupling, they cannot be assigned with certitude to individual members of the mixed anion series.

Table 2. Summary of Crystal Data and Refinement Results for $Te(OTeF_5)_4$ and $N(CH_3)_4^+Te(OTeF_5)_5^-$

	compound	
	$Te(OTeF_5)_4$	$N(CH_3)_4^+Te(OTeF_5)_5^-$
chem formula	$O_4F_{20}Te_5$	$C_4H_{12}NO_5F_{25}Te_6$
space group (No.)	$P\bar{1}$ (2)	*Pbca* (61)
a (Å)	9.502(3)	11.021(2)
b (Å)	9.748(5)	20.096(5)
c (Å)	10.603(4)	27.497(5)
α (deg)	85.73(4)	90
β (deg)	72.50(3)	90
γ (deg)	71.26(3)	90
V (Å^3)	886.7(6)	6090(2)
molecules/unit cell	2	8
mol wt (g mol^{-1})	1082.0	1394.7
calcd density (g cm^{-3})	4.052	3.042
T (°C)	−97	24
μ (cm^{-1})	4.40	58.43
wavelength (Å) used for data collcn	0.56806	0.71073
final agreement factors[a]	$R_1 = 0.0239$ $wR_2 = 0.0577$	$R_1 = 0.1044$ $R_w = 0.0781$

[a] R_1 is defined as $\sum||F_o| - |F_c||/\sum|F_o|$. R_w is defined as $[\sum[w(|F_o| - |F_c|)^2]/\sum w(|F_o|)^2]^{1/2}$. wR_2 is defined as $[\sum[w(F_o^2 - F_c^2)^2)]/\sum w(F_o^2)^2]^{1/2}$.

X-ray Crystal Structures of $Te(OTeF_5)_4$ and $N(CH_3)_4^+Te(OTeF_5)_5^-$. Details of the data collection parameters and other crystallographic information are given in Table 2. The final atomic coordinates and the equivalent isotropic thermal param-

eters are summarized in Table 3. Important bond lengths and angles for $Te(OTeF_5)_4$ and the $Te(OTeF_5)_5^-$ anion and long contacts in $Te(OTeF_5)_4$ are listed in Table 4.

$Te(OTeF_5)_4$. The solid state geometry of $Te(OTeF_5)_4$ is in accord with the gross geometry deduced from a previous low-temperature solution ^{19}F and ^{125}Te NMR study.[2] While several examples of $Te^{IV}-F$ bonds that have been characterized by X-ray crystallography are known,[10,21,22] $F_2Te(OTeF_5)_2$, in $O{=}Re(OTeF_5)_4{\cdot}F_2Te(OTeF_5)_2$,[13] is the only other example of an $OTeF_5$ group bonded to Te^{IV} that has been characterized by X-ray crystallography. Both $Te(OTeF_5)_4$ and $F_2Te(OTeF_5)_2$ are, in the VSEPR[30] notation, AX_4E systems exhibiting the expected disphenoidal geometries. The two axial positions of $Te(OTeF_5)_4$ are occupied by $OTeF_5$ groups, and the equatorial positions are occupied by two $OTeF_5$ groups and a lone electron pair (Figure 3a) whereas both the axial and the equatorial positions of $F_2Te(OTeF_5)_2$ are occupied by one F atom and one $OTeF_5$ group.

Both $F_2Te(OTeF_5)_2$ and $Te(OTeF_5)_4$ exhibit axial and equatorial $O(F)-Te^{IV}-O$ angles that are significantly compressed from their respective ideal angles of 180 and 120° and may be attributed to the stereochemical activity of the lone electron pair and its repulsive interactions with axial and equatorial bond pair domains. The axial angles of both structures are bent toward the two equatorial ligand atoms and away from the sterically active lone electron pair in the equatorial plane [O(1)−Te(1)−O(2), 168.73(9)°, and $O_{ax}-Te-F_{ax}$, 166.4(2)°]. Larger compressions are observed for the equatorial angles [O(3)−Te(1)−O(4), 95.16(12)°, and $O_{eq}-Te-F_{eq}$, 93.3(3)°]. The large compressions for both angles follow the general trend of increasing compression with increasing row in the Periodic Table.[30] The axial $Te^{IV}-O$ bond lengths of $Te(OTeF_5)_4$ [Te(1)−O(1), 1.998(3), and Te(1)−O(2), 2.057(3) Å] are longer than the equatorial bond lengths [Te(1)−O(4), 1.885(2), and Te(1)−O(3), 1.888(3) Å] and are similar to the $Te^{IV}-O_{ax}$ (1.945(6) Å) and $Te^{IV}-O_{eq}$ (1.881(7) Å) bond lengths of $F_2Te(OTeF_5)_2$, reflecting the reduced crowding in the equatorial plane.

The $Te^{VI}-O$ (1.834(3)−1.882(3) Å) and $Te^{VI}-F$ (1.805(2)−1.858(3) Å) bond lengths are in agreement with other known values,[3] and the angles around the tellurium atoms deviate by a maximum of 4° from the ideal octahedral geometry. As a consequence of maintaining the total bond valence[31] of oxygen, the $Te^{VI}-O$ bond lengths reflect the difference in $Te^{IV}-O_{ax}$ and $Te^{IV}-O_{eq}$ bond lengths so that the $Te^{VI}-O_{ax}$ bond lengths (1.834(3) Å) are significantly shorter than the $Te^{VI}-O_{eq}$ bond lengths (1.879(3) Å) and are comparable to those observed in $F_2Te(OTeF_5)_2$ [ax, 1.852(5) Å; eq, 1.876(6) Å] and exhibit a similar relationship between $Te^{VI}-O$ and $Te^{IV}-O$ bond lengths.

Two short contacts exist between Te(1) and two equatorial fluorine atoms, F(2) and F(6), belonging to two axial $OTeF_5$ groups of two different nearest neighbor $Te(OTeF_5)_4$ molecules (Figure 3b). The contacts, Te(1)···F(2b), 2.776 Å, and Te(1)···F(6a), 2.820 Å, are significantly less than the van der Waals sum for Te and F (3.55[32] −3.60[33] Å) and occur trans to the oxygens of the equatorial $OTeF_5$ groups but are displaced by 0.485 (F(6a)) and 0.553 Å (F(2b)) from the equatorial O(3),Te(1),O(4) plane toward the axial O(1) atom, providing a distorted octahedral (AX_4Y_2E) arrangement of four primary oxygen bonds and two secondary fluorine bridge bonds to Te(1)

(30) Gillespie, R. J.; Hargittai, I. *The VSEPR Model of Molecular Geometry*; Allyn and Bacon: Needham Heights, MA, 1991; pp 145−146.
(31) Brown, I. D. *J. Solid State Chem.* **1974**, *11*, 214.
(32) Pauling, L. *The Nature of the Chemical Bond*, 3rd ed.; Cornell University Press: Ithaca, NY, 1960; p 260.
(33) Bondi, A. *J. Phys. Chem.* **1964**, *68*, 441.

Table 3. Atomic Coordinates (×10[4]) and Equivalent Isotropic Displacement Coefficients (Å[2] × 10[3]) for $Te(OTeF_5)_4$ and $N(CH_3)_4^+Te(OTeF_5)_5^-$

	x	*y*	*z*	*U*(eq)[a]
		$Te(OTeF_5)_4$		
Te(1)	76(1)	2473(1)	3534(1)	16(1)
O(1)	−1328(3)	4333(3)	4485(2)	22(1)
Te(2)	−2489(1)	6147(1)	4146(1)	20(1)
F(1)	−761(3)	6594(3)	3166(3)	45(1)
F(2)	−2283(3)	6862(3)	5621(3)	34(1)
F(3)	−4290(3)	5910(3)	5182(3)	36(1)
F(4)	−2766(3)	5561(3)	2671(2)	41(1)
F(5)	−3605(3)	7976(3)	3875(3)	37(1)
O(2)	1382(3)	745(2)	2242(2)	21(1)
Te(3)	2677(1)	−972(1)	2634(1)	21(1)
F(6)	1067(3)	−1224(3)	4046(2)	40(1)
F(7)	2197(3)	−1999(2)	1563(2)	32(1)
F(8)	4362(3)	−844(3)	1311(3)	40(1)
F(9)	3180(3)	−60(3)	3807(3)	44(1)
F(10)	3870(3)	−2670(3)	3099(3)	39(1)
O(3)	627(3)	3618(3)	2068(2)	23(1)
Te(4)	2471(1)	3788(1)	861(1)	20(1)
F(11)	1288(3)	5349(2)	207(2)	32(1)
F(12)	2349(3)	2612(3)	−311(2)	32(1)
F(13)	3667(3)	2253(2)	1553(2)	28(1)
F(14)	2634(3)	4958(2)	2023(2)	34(1)
F(15)	4217(3)	3987(3)	−326(3)	37(1)
O(4)	−1702(3)	2353(3)	3165(3)	23(1)
Te(5)	−2295(1)	1385(1)	2049(1)	20(1)
F(16)	−3485(3)	3102(3)	1622(3)	35(1)
F(17)	−3936(3)	1291(3)	3441(2)	34(1)
F(18)	−1145(3)	−360(2)	2473(3)	33(1)
F(19)	−664(3)	1485(3)	635(2)	31(1)
F(20)	−2919(3)	469(3)	1000(3)	39(1)
		$N(CH_3)_4^+Te(OTeF_5)_5^-$		
Te(1)	2546(2)	1058(1)	6539(1)	79(1)
O(1)	3882(28)	1454(15)	6211(11)	145(11)
Te(2)	4970(3)	1604(2)	5790(1)	105(1)
F(1)	4414(29)	2447(14)	5722(10)	197(17)
F(2)	5875(30)	1901(18)	6279(13)	235(21)
F(3)	5535(26)	834(17)	5817(10)	193(16)
F(4)	4212(24)	1325(14)	5258(10)	163(14)
F(5)	6160(29)	1814(21)	5391(12)	271(24)
O(2)	2574(30)	1823(18)	6971(12)	187(13)
Te(3)	2973(5)	2621(2)	7182(2)	143(2)
F(6)	2691(64)	2393(19)	7759(16)	368(39)
F(7)	1741(50)	2954(24)	7195(25)	361(40)
F(8)	3361(58)	2901(19)	6635(20)	381(40)
F(9)	4371(55)	2315(26)	7385(31)	420(51)
F(10)	3327(44)	3401(18)	7413(17)	326(31)
O(3)	4107(36)	645(20)	6913(14)	220(17)
Te(4)	4704(3)	298(2)	7369(1)	111(1)
F(11)	5640(41)	951(29)	7443(22)	423(43)
F(12)	3776(37)	666(25)	7819(12)	313(31)
F(13)	3734(44)	−304(19)	7405(22)	443(39)
F(14)	5624(42)	−132(26)	6984(13)	367(31)
F(15)	5359(42)	−43(24)	7837(15)	282(19)
O(4)	2988(32)	330(20)	6017(14)	212(16)
Te(5)	2481(3)	−403(2)	5760(1)	108(1)
F(16)	1608(67)	−54(18)	5327(16)	412(48)
F(17)	1458(51)	−499(26)	6231(22)	437(42)
F(18)	3436(57)	−832(22)	6120(25)	404(42)
F(19)	3345(58)	−342(28)	5253(23)	365(42)
F(20)	2180(25)	−1175(14)	5470(12)	195(17)
O(5)	1563(47)	1471(25)	6031(18)	278(21)
Te(6)	197(4)	1804(2)	5813(2)	129(2)
F(21)	−25(51)	2219(31)	6292(19)	421(39)
F(22)	−352(55)	1147(22)	6000(25)	501(51)
F(23)	471(38)	1488(26)	5311(15)	315(28)
F(24)	732(67)	2555(22)	5636(23)	382(48)
F(25)	−1096(40)	2197(26)	5559(19)	347(36)
N(1)	7344(30)	1009(16)	1024(11)	103(10)
C(1)	7222(35)	336(20)	1143(16)	150
C(2)	6907(37)	1298(21)	1441(14)	150
C(3)	8540(35)	1162(21)	1101(15)	150
C(4)	6459(37)	1280(21)	700(14)	150

[a] Equivalent isotropic *U* defined as one-third of the trace of the orthogonalized U_{ij} tensor.

Table 4. Bond Lengths and Bond Angles in $Te(OTeF_5)_4$ and $N(CH_3)_4^+Te(OTeF_5)_5^-$ and Long Contacts for $Te(OTeF_5)_4$

Bond Lengths and Long Contacts (Å) for $Te(OTeF_5)_4$

Te(1)−O(1)	1.998(3)	Te(2)−F(4)	1.822(2)	Te(4)−O(3)	1.882(3)	Te(5)−F(16)	1.807(2)
Te(1)−O(2)	2.057(3)	Te(2)−F(5)	1.810(2)	Te(4)−F(11)	1.809(2)	Te(5)−F(17)	1.817(2)
Te(1)−O(3)	1.888(3)	Te(3)−O(2)	1.835(2)	Te(4)−F(12)	1.805(2)	Te(5)−F(18)	1.810(2)
Te(1)−O(4)	1.885(2)	Te(3)−F(6)	1.858(3)	Te(4)−F(13)	1.820(2)	Te(5)−F(19)	1.827(2)
Te(2)−O(1)	1.834(3)	Te(3)−F(7)	1.809(2)	Te(4)−F(14)	1.811(2)	Te(5)−F(20)	1.809(2)
Te(2)−F(1)	1.825(3)	Te(3)−F(8)	1.816(3)	Te(4)−F(15)	1.814(2)	Te(1)···F(2b)	2.776(2)
Te(2)−F(2)	1.845(2)	Te(3)−F(9)	1.833(2)	Te(5)−O(4)	1.875(2)	Te(1)···F(6a)	2.820(2)
Te(2)−F(3)	1.810(2)	Te(3)−F(10)	1.811(2)				

Bond Angles (deg) for $Te(OTeF_5)_4$

Te(1)−O(1)−Te(2)	140.03(14)	Fe(5)−Te(2)−F(2)	88.59(12)	Fe(6)−Te(3)−F(9)	87.34(14)	F(12)−Te(4)−F(14)	178.85(11)
Te(1)−O(2)−Te(3)	125.84(13)	F(1)−Te(2)−F(2)	88.25(14)	F(7)−Te(3)−F(8)	90.96(13)	F(13)−Te(4)−F(14)	88.34(11)
Te(1)−O(3)−Te(4)	137.07(14)	−F(3)	173.70(11)	−F(9)	175.29(12)	O(4)−Te(5)−F(16)	89.94(12)
Te(1)−O(4)−Te(5)	141.46(14)	−F(4)	91.6(2)	F(8)−Te(3)−F(9)	91.32(14)	−F(17)	88.64(11)
O(4)−Te(1)−O(3)	95.16(12)	F(2)−Te(2)−F(3)	88.06(12)	O(3)−Te(4)−F(11)	88.01(11)	−F(18)	91.49(12)
O(4)−Te(1)−O(1)	85.47(11)	−F(4)	176.25(11)	−F(12)	90.51(12)	−F(19)	92.03(11)
O(3)−Te(1)−O(1)	86.35(11)	F(3)−Te(2)−F(4)	91.78(13	−F(13)	92.07(11)	−F(20)	178.53(12)
O(4)−Te(1)−O(2)	88.29(10)	O(2)−Te(3)−F(6)	90.77(12)	−F(14)	90.53(12)	F(16)−Te(5)−F(17)	89.42(13)
O(3)−Te(1)−O(2)	84.87(11)	−F(7)	92.19(11)	−F(15)	178.47(11)	−F(18)	178.29(10)
O(1)−Te(1)−O(2)	168.73(9)	−F(8)	93.89(12)	F(15)−Te(4)−F(11)	90.49(12)	−F(19)	90.06(13)
O(1)−Te(2)−F(1)	92.24(12)	−F(9)	91.76(12)	−F(12)	89.22(12)	−F(20)	89.39(12)
−F(2)	89.43(11)	−F(10)	176.92(12)	−F(13)	89.44(12)	F(17)−Te(5)−F(18)	89.68(12)
−F(3)	92.83(12)	F(10)−Te(3)−F(6)	86.17(13)	−F(14)	89.76(12)	−F(19)	179.15(11)
−F(4)	94.32(11)	−F(7)	88.14(12)	F(11)−Te(4)−F(12)	90.56(12)	−F(20)	90.05(12)
−F(5)	177.03(11)	−F(8)	89.16(13)	−F(13)	178.30(11)	F(18)−Te(5)−F(19)	90.82(12)
F(5)−Te(2)−F(1)	87.10(13)	−F(9)	87.78(12)	−F(14)	89.96(12)	−F(20)	89.16(12)
−F(2)	87.66(12)	F(6)−Te(3)−F(7)	90.05(13	F(12)−Te(4)−F(13)	91.14(11)	F(19)−Te(5)−F(20)	89.28(12)
−F(3)	87.65(13)	−F(8)	175.19(12)				

Bond Lengths (Å)[a] for $N(CH_3)_4^+Te(OTeF_5)_5^-$

Te(1)−O(1)	1.90(3)	Te(2)−F(4)	1.78(3) [1.79]	Te(4)−F(11)	1.68(5) [1.86]	Te(5)−F(19)	1.69(6) [1.88]
−O(2)	1.94(4)	−F(5)	1.76(3) [1.78]	−F(12)	1.77(4) [1.92]	−F(20)	1.78(3) [1.79]
−O(3)	2.17(4)	Te(3)−O(2)	1.76(4)	−F(13)	1.62(4) [1.79]	Te(6)−O(5)	1.75(5)
−O(4)	2.11(4)	−F(6)	1.68(5) [1.83]	−F(14)	1.70(5) [1.84]	−F(21)	1.58(5) [1.72]
−O(5)	1.95(5)	−F(7)	1.52(5) [1.63]	−F(15)	1.63(4)	−F(22)	1.54(6) [1.69]
Te(2)−O(1)	1.69(3)	−F(8)	1.66(5) [1.82]	Te(5)−O(4)	1.73(4)	−F(23)	1.55(4) [1.68]
−F(1)	1.81(3) [1.84]	−F(9)	1.75(6) [1.91]	−F(16)	1.68(6) [1.88]	−F(24)	1.69(5) [1.85]
−F(2)	1.78(4) [1.79]	−F(10)	1.74(4) [1.77]	−F(17)	1.73(6) [1.92]	−F(25)	1.77(5) [1.80]
−F(3)	1.67(3) [1.70]	Te(4)−O(3)	1.58(4)	−F(18)	1.68(6) [1.87]		

Bond Angles (deg) for $N(CH_3)_4^+Te(OTeF_5)_5^-$

Te(1)−O(1)−Te(2)	161(2)	F(2)−Te(2)−F(3)	94(2)	O(3)−Te(4)−F(14)	89(2)	F(20−Te(5)−F(19)	78(2)
−O(2)−Te(3)	158(2)	F(3)−Te(2)−F(4)	85(1)	O(3)−Te(4)−F(15)	178(2)	F(16)−Te(5)−F(17)	102(3)
−O(3)−Te(4)	151(2)	F(4)−Te(2)−F(1)	93(1)	F(15)−Te(4)−F(11)	88(3)	F(17)−Te(5)−F(18)	85(3)
−O(4)−Te(5)	143(2)	O(2)−Te(3)−F(6)	91(2)	−F(12)	83(2)	F(18)−Te(5)−F(19)	100(3)
−O(5)−Te(6)	152(3)	−F(7)	101(2)	−F(13)	86(3)	F(19)−Te(5)−F(16)	73(3)
O(1)−Te(1)−O(2)	87(1)	−F(8)	94(2)	−F(14)	91(2)	O(5)−Te(6)−F(21)	93(3)
−O(3)	77(1)	−F(9)	90(2)	F(11)−Te(4)−F(12)	87(3)	−F(22)	84(3)
−O(4)	78(1)	−F(10)	177(2)	F(12)−Te(4)−F(13)	84(3)	−F(23)	89(2)
−O(5)	85(2)	F(10)−Te(3)−F(6)	87(2)	F(13)−Te(4)−F(14)	93(3)	−F(24)	98(3)
O(1)−Te(2)−F(1)	90(1)	−F(7)	78(3)	F(14)−Te(4)−F(11)	96(3)	−F(25)	174(2)
−F(2)	87(2)	−F(8)	88(2)	O(4)−Te(5)−F(16)	97(2)	F(25)−Te(6)−F(21)	88(3)
−F(3)	94(1)	−F(9)	90(3)	−F(17)	90(2)	−F(22)	101(3)
−F(4)	100(1)	F(6)−Te(3)−F(7)	86(3)	−F(18)	90(2)	F(25)−Te(6)−F(23)	89(2)
−F(5)	175(2)	F(7)−Te(3)−F(8)	96(3)	−F(19)	95(2)	−F(24)	77(3)
F(5)−Te(2)−F(1)	88(2)	F(8)−Te(3)−F(9)	101(3)	O(4)−Te(5)−F(20)	172(2)	F(21)−Te(6)−F(22)	97(3)
−F(2)	88(2)	F(9)−Te(3)−F(6)	77(4)	F(20)−Te(5)−F(16)	87(2)	F(22)−Te(6)−F(23)	91(3)
−F(3)	88(2)	O(3)−Te(4)−F(11)	90(3)	−F(17)	97(2)	F(23)−Te(6)−F(24)	92(3)
−F(4)	85(1)	−F(12)	98(2)	−F(18)	86(2)	F(24)−Te(5)−F(21)	80(3)
F(1)−Te(2)−F(2)	87(2)	−F(13)	96(2)				

[a] Distances after corrections for thermal motion by the riding model are given in brackets.

(Figure 3b). The bridging $Te^{VI}-F_{eq}$ bond lengths, Te(2)−F(2), 1.845(2), and Te(3)−F(6), 1.858(3) Å, are correspondingly longer than the nonbridging $Te^{VI}-F_{eq}$ bond lengths which range from 1.805(2) to 1.833(2) Å. The approaches of the bridging fluorines on the same side of the equatorial O(3),Te(1),O(4) plane is consistent with displacement of the lone electron pair from the equatorial plane of the AX_4E arrangement toward the pseudotrigonal face defined by F(2b),F(6a),O(2). This face contains the sterically active lone electron pair and is splayed open relative to the pseudotrigonal face defined by O(1),O(3),O(4) as a result of lone electron pair−bond pair repulsions which also account for unequal $Te^{IV}-O_{ax}$ bond lengths, so that the Te−O bond pair domain proximate to the lone electron pair, Te(1)−O(2), is elongated relative to Te(1)−O(1). The geometry resembles a distorted octahedral arrangement akin to that of XeF_6[34] (AX_6E) and is most closely related to that of the AX_4Y_2E VSEPR arrangement of the $XeOF_3^+$ cation in $XeOF_3^+SbF_6^-$,[35]

(34) (a) Cutler, J. N.; Bancroft, G. M.; Bozek, J. D.; Tan, K. H.; Schrobilgen, G. J. *J. Am. Chem. Soc.* **1991**, *113*, 9125. (b) Rothman, M. J.; Bartell, L. S.; Ewig, C. S.; van Wazer, J. R. *J. Chem. Phys.* **1980**, *73*, 375. (c) Pitzer, K. S.; Bernstein, L. S. *J. Chem. Phys.* **1975**, *63*, 3849 and references therein.

(35) Mercier, H. P. A.; Sanders, J. C. P.; Schrobilgen, G. J.; Tsai, S. S. *Inorg. Chem.* **1993**, *32*, 386.

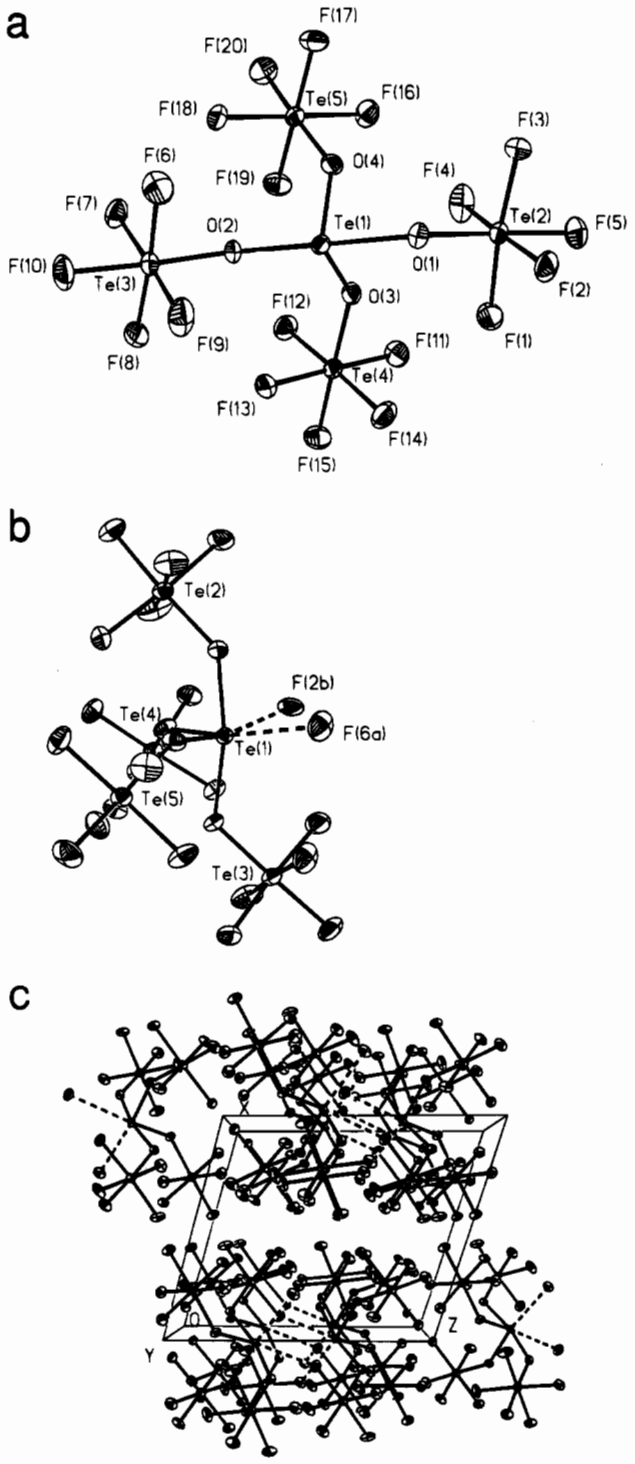

Figure 3. ORTEP views showing (a) the asymmetric unit of the crystal structure of $Te(OTeF_5)_4$, (b) the two secondary $Te^{IV}\cdots F$ contacts (thermal ellipsoids shown at the 50% probability level), and (c) a ball and stick diagram of the resulting parallel chains defining a layer running parallel to the *b*-axis and the $Te^{IV}\cdots F$ contacts.

with two secondary contacts between the central Xe atom and a fluorine atom from each of two SbF_6^- anions.

The relative conformations of the equatorial and axial $OTeF_5$ groups are likely a consequence of the secondary fluorine bridge bonding to the central Te^{IV} atom. The axial $O(1)Te(2)F_5$ group is bent away from the neighboring axial $OTeF_5$ groups that contribute the long fluorine contacts with the central Te^{IV} atom (*vide supra*), and in turn, the equatorial $OTeF_5$ groups are bent toward the axial $O(2)Te(3)F_5$ group and away from the axial $O(1)Te(2)F_5$ group, giving axial $OTeF_5$ group conformations which are syn and anti, respectively, to the lone electron pair.

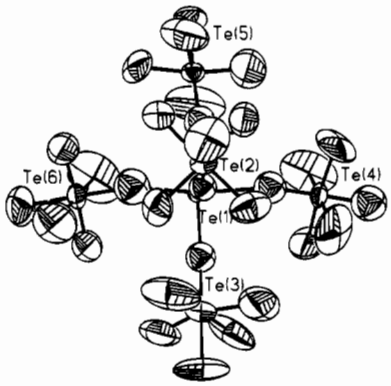

Figure 4. ORTEP view of the $Te(OTeF_5)_5^-$ anion showing the numbering of the atoms. Thermal ellipsoids are shown at the 20% probability level.

The shortest intramolecular F···F contacts range from 2.658 to 3.025 Å (average, 2.949 Å). The closest intermolecular F···F contacts between the equatorial and axial $OTeF_5$ groups occur for $O(1)Te(2)F_5$ at F(4)···F(16), 3.058 Å, and F(1)···F(11), 3.238 Å, and for $O(2)Te(3)F_5$ at F(6)···F(18), 2.944 Å, F(8)···F(13), 2.890 Å, F(7)···F(18), 2.948 Å, and F(9)···F(13), 3.196 Å. Both intramolecular and intermolecular F···F contacts are somewhat greater than the sum of the van der Waals radii for fluorine, 2.70[32]–2.80[33] Å, indicating that there is little in the way of $OTeF_5\cdots OTeF_5$ steric interactions as a result of the conformation assumed by $Te(OTeF_5)_4$. The shortest intramolecular Te(1)···F contacts occur for $O(2)Te(3)F_5$ [Te(1)···F(9), 3.256 Å, and Te(1)···F(6), 3.464 Å] and are close to the sum of the van der Waals radii for Te and F (3.55 Å), straddling the lone electron pair position and the pseudotrigonal face it occupies.

Like its extensively fluorine-bridged analog, TeF_4, $Te(OTeF_5)_4$ may be described as a polymeric chain structure. The secondary contacts to Te^{IV}, Te(1)···F(2b) and Te(1)···F(6a), result in the distorted octahedral AX_4Y_2E geometry about Te^{IV} discussed above and are bridged through axial $OTeF_5$ groups along the *c*-axis of the unit cell. Two parallel chains result (Figure 3c) which define a layer running parallel to the *b*-axis such that the lone electron pairs of each chain are directed toward the interior of a channel defined by the two parallel chains (Supporting Information Figure 8). The closest fluorine–fluorine distances between adjacent layers occur at 2.900 Å along the *c*-axis and at 2.929 Å along the *a*-axis.

$N(CH_3)_4^+Te(OTeF_5)_5^-$. The structure of $N(CH_3)_4^+Te(OTeF_5)_5^-$ consists of well-separated anions and cations. The central Te^{IV} atom in the $Te(OTeF_5)_5^-$ anion is coordinated to five crystallographically nonequivalent $OTeF_5$ groups, so that the gross geometry can be described as either a distorted square pyramid or as a pseudo-octahedron if the sterically active free valence electron pair on Te^{IV} is included as a sixth ligand (Figure 4). The tetramethylammonium cation is tetrahedral about nitrogen with the expected bond lengths and bond angles.[3]

The five $OTeF_5$ groups of the anion have ample space and, therefore, do not suffer any significant distortion from their normal pseudo-octahedral geometry. All distances between atoms of neighboring $OTeF_5$ groups are longer than the sums of the corresponding van der Waals radii for two fluorines (2.70[32]–2.80[33] Å) and for an oxygen and a fluorine (2.75[32]–2.80[33] Å) as well as the closest contacts within $OTeF_5$ groups, F···F, 2.211–2.479 Å, and F···O, 2.211–2.454 Å. The closest intermolecular F···F and F···O contacts between different $OTeF_5$ groups are as follows: $OTe(2)F_5\cdots OTe(3)F_5$, F(1)···F(8) = 2.910 Å; $OTe(2)F_5\cdots OTe(5)F_5$, F(4)···F(19) = 3.483 Å, F(3)···O(4) = 3.034 Å, and F(4)···O(4) = 3.191 Å.

As noted in both published structures of the $Sb(OTeF_5)_6^-$ anion[3] and in the $U(OTeF_5)_6$ molecule,[36] the fluorine and oxygen atoms have exceptionally large thermal parameters showing that the pentafluorotellurate groups are undergoing librational motions of large amplitude, a problem which was enhanced by our inability to obtain a crystal structure at low temperature owing to a phase transition (see **Experimental Section**). A standard rigid-body librational analysis was performed. As already noted in related compounds, the Te−O and Te−F (especially $Te-F_{eq}$) distances are significantly affected by thermal motion and, as expected, the librationally corrected Te−F bond distances are longer than the uncorrected distances (Table 4) and are in good agreement with other known values (average Te−F = 1.81 Å). With a lack of anisotropic parameters for the basal oxygen atoms, no corrected values for the $Te^{IV}-O$ and $Te^{VI}-O$ bond lengths are reported.

The immediate environment around the Te^{IV} atom of the $Te(OTeF_5)_5^-$ anion is that predicted by the VSEPR rules for a pseudo-octahedral AX_5E system[30] and is in accord with the gross geometry deduced from solution ^{19}F and ^{125}Te NMR spectroscopy (**NMR Spectroscopy of $Te(OTeF_5)_5^-$ and $FTe(OTeF_5)_4^-$ Anions**). The local $Te^{IV}O_5$ geometry of $Te(OTeF_5)_5^-$ closely resembles that of its fluorine analog, TeF_5^- in $N(CH_3)_4^+TeF_5^-$ [16] and $K^+TeF_5^-$.[18] The $Te-O_{ax}$ (1.90(3) Å) and $Te-O_{eq}$ (1.94(4)–2.17(4); average, 2.04(4) Å) bond length differences are similar to those encountered for TeF_5^- in $K^+TeF_5^-$ ($Te-F_{ax}$, 1.862(4) Å; $Te-F_{eq}$, 1.953(4) Å) and $N(CH_3)_4^+TeF_5^-$ ($Te-F_{ax}$, 1.859(6) Å; $Te-F_{eq}$, 1.949(6) Å) and are a consequence of the lone pair–bond pair repulsions which cause lengthening of the equatorial bonds compared with the axial bond. The $Te^{IV}-O_{eq}$ bond lengths of $Te(OTeF_5)_5^-$ are similar to the more sterically crowded $Te^{IV}-O_{ax}$ bond lengths in $Te(OTeF_5)_4$ (average, 2.022(3) Å) and in $F_2Te(OTeF_5)_2$ (1.945(6) Å). Moreover, the less sterically congested $Te^{IV}-O_{ax}$ bond length of $Te(OTeF_5)_5^-$ is similar to the less sterically congested equatorial bond lengths of $Te(OTeF_5)_4$ (average, 1.887(3) Å) and $F_2Te(OTeF_5)_2$ (1.881(7) Å). The $Te^{IV}-O_{eq}$ bonds of $Te(OTeF_5)_5^-$ are tilted away from the lone pair as a result of lone pair–bond pair repulsions so that the $O_{ax}-Te-O_{eq}$ angles are compressed from the ideal 90° angle to an average angle of 81° (range, 77(1)–86(1)°), in close agreement with the $F_{ax}-Te-F_{eq}$ angle observed in TeF_5^- ($K^+TeF_5^-$, 78.9(2)°;[18] $N(CH_3)_4^+TeF_5^-$, 80.7° [16]).

Unlike the structurally related pseudo-octahedral and square planar main-group and square pyramidal transition metal $OTeF_5$ derivatives (*vide infra*) studied to date, the four equatorial oxygen atoms and the Te^{IV} atom of $Te(OTeF_5)_5^-$ are not coplanar. Displacement of the central Te(1) atom from the equatorial plane of oxygen atoms is best described with respect to an average equatorial plane. Calculation of the mean least-squares plane[37] passing through O(2), O(3), O(4), and O(5) and perpendicular to the Te(1)–O(1) direction shows that the equatorial oxygen atoms are coplanar within experimental error. As expected for a molecule possessing an AX_5E geometry, the $O_{ax}-Te^{IV}-O_{eq}$ angles are smaller than 90° and the central Te^{IV} atom is found to be displaced below the average plane defined by the equatorial oxygen atoms. The displacement of the Te^{IV} atom from the basal plane is −0.30 Å and is similar to that calculated in both structures of the TeF_5^- anion ($K^+TeF_5^-$, −0.377 Å; $N(CH_3)_4^+TeF_5^-$, −0.326 Å). Several other structures of ionic and neutral pseudo-octahedral main-group and square pyramidal transition metal $OTeF_5$ derivatives have been previously determined. In the case of $Xe(OTeF_5)_4$[20] and $I(OTeF_5)_4^-$,[19] both axial positions are occupied by lone electron pairs, while for $O{=}I(OTeF_5)_4^-$ [19] and $O{=}M(OTeF_5)_4$ (M = Mo,[21,22] W,[22] Re,[13] Os[21]), one of the apical positions is occupied by an oxygen atom doubly bonded to the central heavy atom and is trans to either a lone electron pair, as in the case of $O{=}I(OTeF_5)_4^-$, or is vacant, as in the case of the transition metal analogs. In all three types of compounds, the four oxygens belonging to the $OTeF_5$ groups are coplanar, while the position of the central atom relative to the equatorial oxygen plane is variable. For $O{=}I(OTeF_5)_4^-$, the iodine atom was found to lie, within 3σ, in the O_4 plane (actually 0.018(5) Å above the plane). The iodine atom is coplanar with the four oxygen atoms as in $I(OTeF_5)_4^-$ and $Xe(OTeF_5)_4$ because the steric requirements of an oxygen double bond are similar to those of a lone electron pair. The Mo, W, Re, and Os atoms were found to be displaced above their respective planes by 0.419 and 0.385, 0.403, 0.348, and 0.267 Å, respectively. The square pyramidal shapes of the transition metal derivatives are basically determined by d-orbital participation in the bonding to the oxygens, and the positioning of the transition metal atoms above the plane is a consequence of no free electron pair having a high s-character in the axial position and may serve to relieve $Te^{IV}-O\cdots Te^{IV}-O$ bond pair interactions.

All three types of the aforementioned $OTeF_5$ derivatives have adjacent $OTeF_5$ groups pointing pairwise up and down (trans-anti) with respect to the equatorial MO_4 plane. No satisfactory explanation, however, has been advanced for why *trans, anti*-conformations are preferred over *trans, syn*-conformations. In $EYX(OTeF_5)_4$ and *trans*-$F_2Te(OTeF_5)_4$ compounds where Y is the axial ligand and cylindrical, i.e., a free electron pair or F, the four $OTeF_5$ ligands should alternate up and down. Only if Y is replaced by a noncylindrical $OTeF_5$ group may *trans-anti*-structures become more favorable. It is noteworthy that *trans*-$F_2Te(OTeF_5)_4$[38] is the only example where $OTeF_5$ groups alternate up and down so that the *trans*-$OTeF_5$ groups are syn to one another. The conformational energy differences might be small, and the observed *trans-anti*-conformations may result from the effects of crystal packing. The $Te(OTeF_5)_5^-$ anion is the first example of a pseudo-octahedral $OTeF_5$ compound in which the axial position is occupied by a noncylindrical group and which has been structurally characterized by X-ray crystallography. As a consequence of the steric effect of the axial $OTeF_5$ group, the relative conformations of the equatorial $OTeF_5$ groups differ markedly from those of other known $OTeF_5$ derivatives having AX_5E and AX_4E_2 geometries. The relative $OTeF_5$ conformations of the $Te(OTeF_5)_5^-$ anion are closely related to the *trans, syn*-$OTeF_5$ and *cis, anti*-$OTeF_5$ conformations observed in *trans*-$F_2Te(OTeF_5)_4$. Figure 5a,b represents two views perpendicular to the [O(1), O(2), O(4)] and the [O(1), O(3), O(5)] planes, respectively, of the $Te(OTeF_5)_5^-$ anion. The axial $OTe(2)F_5$ group points toward the equatorial $OTe(5)F_5$ group, which, in turn, is directed away from the $OTe(2)F_5$ group. The two $OTeF_5$ groups are not, however, perfectly eclipsed (Figure 4). The two equatorial *trans*-$OTeF_5$ groups, $OTe(4)F_5$ and $OTe(6)F_5$, are cis to $OTe(5)F_5$ and also point away from the apical $OTe(2)F_5$ group so that they adopt a *trans, syn*-conformation relative to one another. The $OTe(3)F_5$ group trans to $OTe(5)F_5$ points toward the apical $OTe(2)F_5$ group so that these two equatorial groups have a *trans, anti*-conformational

(36) Templeton, L. K.; Templeton, D. H.; Bartlett, N.; Seppelt, K. *Inorg. Chem.* **1976**, *15*, 2720.

(37) The equation for the equatorial least-squares plane is defined by $7.84x + 10.41y - 13.1z = 5.15$ in the direct crystal coordinate system. It was calculated by the program BESPLN from the NRCVAX package. NRCVAX Crystal Structure System: Larson, A. C.; Lee, F. L.; LePage, Y.; Webster, M.; Charland, J. P.; Gabe, E. J. Chemistry Division, NRC, Ottawa, Canada. PC version: White, P. S. Department of Chemistry, University of North Carolina, Chapel Hill, NC.

(38) (a) Pritzkow, H.; Seppelt, K. *Angew. Chem., Int. Ed. Engl.* **1976**, *15*, 771. (b) Pritzkow, H.; Seppelt, K. *Inorg. Chem.* **1977**, *16*, 2685.

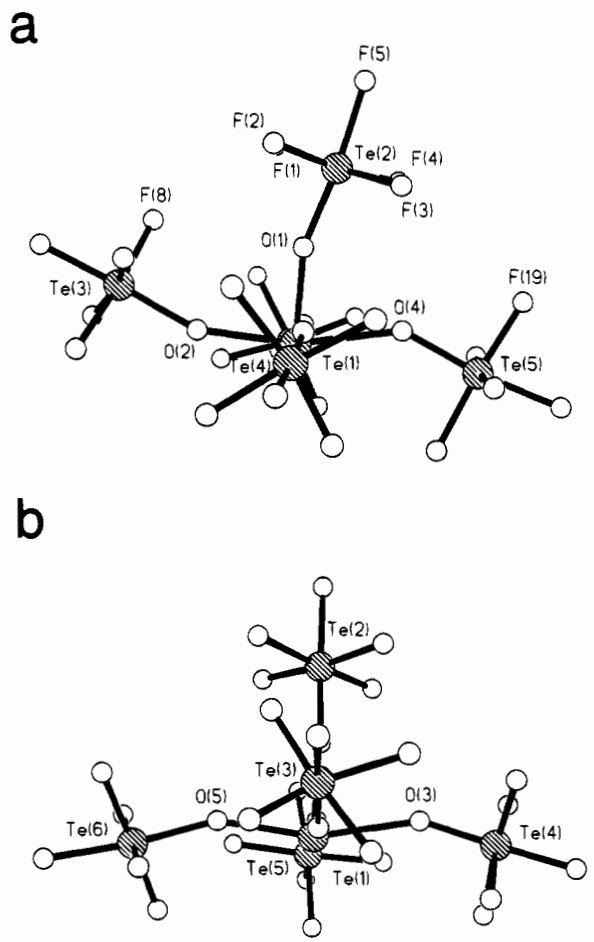

Figure 5. Two views of the $Te(OTeF_5)_5^-$ anion showing the arrangement of the $OTeF_5$ groups perpendicular to (a) the [O(1), O(2), O(4)] and (b) the [O(1), O(3), O(5)] planes.

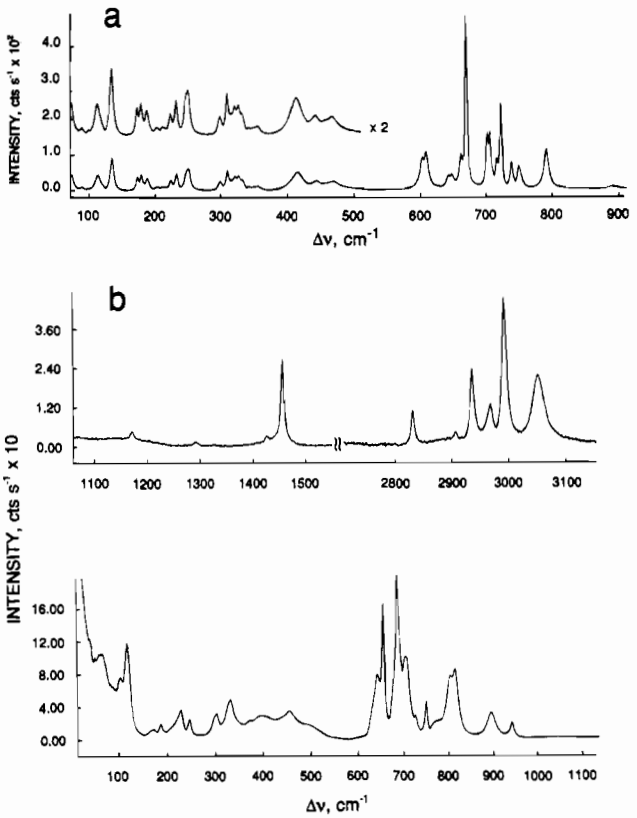

Figure 6. Raman spectra of microcrystalline (a) $Te(OTeF_5)_4$ and (b) $N(CH_3)_4^+Te(OTeF_5)_5^-$ recorded in glass capillaries at room temperature using 514.5-nm excitation.

relationship apparently imposed by $OTe(2)F_5\cdots OTe(5)F_5$ steric interactions. Three $Te^{IV}-O_{eq}-Te^{VI}{}_{eq}$ angles are equal within experimental error, ranging from 151(2) to 158(2)°, and as a result of increased congestion, the fourth angle, Te(1)−O(4)−Te(5), is significantly smaller (143(2)°) (Table 4) and the axial $Te^{IV}-O_{ax}-Te^{VI}{}_{ax}$ angle is more open (161(2)°).

The closest anion−cation contacts occur at 3.015 [F(23)···C(4)], 3.320 [F(14)···C(1)], and 3.399 Å [F(18)···C(3)]. The sum of the van der Waals radii of CH_3 (2.00 Å)[32] and F (1.35[32]−1.40[33] Å) is 3.35−3.40 Å. These short contact distances suggest weak hydrogen bonding between the methyl groups and these three fluorine atoms (see **Raman Spectra of $Te(OTeF_5)_4$ and $N(CH_3)_4^+Te(OTeF_5)_5^-$**). The anions and cations are stacked along the *a*- and *b*-axes so that the layers alternate between two cations and two anions in the *a*-direction and single anions and cations in the *b*-direction (Supporting Information Figure 9). The formal negative charge of the anion is expected to be dispersed over 20 fluorines. The closest contact in the anion···anion pairs, which are packed so that the axial positions occupied by the lone electron pair on each Te^{IV} face one another, is 2.979 Å (F(15)···F(17)). This arrangement serves to maximize the negative charge separation within each anion pair. The presence of a sterically active valence lone electron pair in the sixth coordination position of Te^{IV} in $Te(OTeF_5)_5^-$, along with Coulombic repulsions and orientation of the anions relative to one another, preclude close interanionic contacts, with the shortest $Te^{IV}\cdots$anion contacts at 3.507 (Te(1)···F(11)) and 3.695 Å (Te(1)···F(15)). In contrast, the sixth coordination site of the metal pseudo-octahedron in $O{=}M(OTeF_5)_4$ (M = Mo, W, Re, Os) is not occupied by a lone electron pair and exhibits a short contact with a fluorine atom [$O{=}Mo(OTeF_5)_4$ (Mo···F, 2.59(2)[22] and 2.55(1) Å);[21] $O{=}W(OTeF_5)_4$ (W···F, 2.58(1) Å);[22] $O{=}Re(OTeF_5)_4{\cdot}F_2Te(OTeF_5)_2$ (Re···F, 2.210(5) Å);[13] $O{=}Os(OTeF_5)_4{\cdot}F^-{\cdot}TeF_3^+{\cdot}2TeF_4$ (Os···F, 2.05(2) Å)[21]]. As in the case of iodine in $O{=}I(OTeF_5)_4^-$ (shortest intermolecular contact is I···F, 4.20 Å),[19] the Te^{IV} atom of the $Te(OTeF_5)_5^-$ anion is well insulated from intermolecular interactions, which is, in large measure, related to the packing of the anion along the *a*-axis of the unit cell (*vide supra*).

Raman Spectra of $Te(OTeF_5)_4$ and $N(CH_3)_4^+Te(OTeF_5)_5^-$. The Raman spectra of solid $Te(OTeF_5)_4$ and $N(CH_3)_4^+Te(OTeF_5)_5^-$ are shown in Figure 6. The observed frequencies and their assignments are summarized in Table 5. Spectral assignments are necessarily tentative owing to uncertainties regarding the degree of vibrational coupling among the $OTeF_5$ modes of the ligands, which appears to be weak; the anticipated coupling among vibrational modes associated with the Te−O−Te moieties; site symmetry lowering and vibrational coupling within the unit cell (factor-group splitting). Moreover, it is not possible to distinguish between the vibrational modes of the axial and equatorial $OTeF_5$ groups. The assignments of the frequencies of the $OTeF_5$ groups have been aided by comparison with the most recent assignments for $N(CH_3)_4^+TeOF_5^-$,[39] for which *ab initio* calculations and a normal coordinate analysis confirm the correctness of the assignments, and by assignments for F_5TeOF.[40] Assignments were made under C_{4v} symmetry for the $OTeF_5$ groups with each group contributing 15 vibrations, $4A_1 + 2B_1 + B_2 + 4E$, all of which are formally Raman active (A_1 and E are infrared active), and generally require little further comment. The antisymmetric TeF_4 stretching mode, $\nu_8(E)$, is

(39) Christe, K. O.; Dixon, D. A.; Sanders, J. C. P.; Schrobilgen, G. J.; Wilson, W. W. *Inorg. Chem.* **1993**, *32*, 4089.
(40) Schack, C. J.; Wilson, W. W.; Christe, K. O. *Inorg. Chem.* **1983**, *22*, 18.

Table 5. Raman Frequencies and Assignments for $Te(OTeF_5)_4$ and $N(CH_3)_4^+Te(OTeF_5)_5^-$ [a]

freq, cm^{-1}		assgnts	
$Te(OTeF_5)_4$	$N(CH_3)_4^+Te(OTeF_5)_5^-$	cation (T_d)	anion (C_{4v})
	3053 (10)	$\nu_5(E)$, $\nu_{as}(CH_3)$; $\nu_{13}(T_2)$, $\nu_{as}(CH_3)$	
	2994 (22)	$\nu_1(A_1)$, $\nu_s(CH_3)$	
	2968 (6)	$\nu_{14}(T_2)$, $\nu_{as}(CH_3)$	
	2936 (11)	$2\nu_6(E)$, $2\nu_2(A_1)$	
	2906 (1)	?	
	2831 (5)	$2\nu_{16}(T_2)$	
	1457 (13)	$\nu_2(A_1)$, $\delta(CH_3)$; $\nu_6(E)$, $\delta_{as}(CH_3)$	
	1426 (1)	$\nu_{16}(T_2)$, $\delta_{as}(CH_3)$	
	1291 (<1)	$\nu_{17}(T_2)$, $\delta_{rock}(CH_3)$	
	1171 (1)	$\nu_7(E)$, $\delta_{rock}(CH_3)$	
	952 (10)	$\nu_{18}(T_2)$, $\nu_{as}(CN_4)$	
892 (2)	905 (16)		
	822 (42)		*b*
792 (23)	810 (38)		
	779 (11)	$\nu_3(A_1)$, $\nu_s(CN_4)$	
754 (10), sh	756(23)		$\nu_1(A_1)$, $\nu(TeF)$
750 (14)	731 (14)		
739 (16)	710 (50)		
723 (50)			
716 (18)			
710 (13), sh			
706 (35)			
702 (34)			
671 (100)	691 (100)		$\nu_2(A_1)$, $\nu_s(TeF_4)$
662 (21)	682 (37), sh		
659 (82)			
648 (9)	645 (39)		$\nu_5(B_1)$, $\nu_{as}(TeF_4)$
643 (9)	633 (19), sh		
610 (23)			
604 (19)			
469 (7)	490 (8)		$\nu_3(A_1)$, $\nu(Te^{VI}-O)$ $\nu_{as}(Te^{IV}-O_{eq})$
461 (6)			$\nu_s(Te^{IV}\text{-}O_{eq})$ $\nu_s(Te^{IV}\text{-}O_{ax})$
445 (8)			
416 (14)			
	453 (16)	$\nu_{19}(T_2)$, $\delta(CN_4)$	
	398 (13)	$\nu_8(E)$, $\delta(CN_4)$	
	375 (10)		
355 (4)	335 (22)		$\nu_9(E)$, $\delta(FTeF_4)$
349 (3)			
342 (3)			
332 (8)			
327 (11)			
321 (11)			
316 (8)	307 (14)		$\nu_{10}(E)$, $\delta(OTeF_4)$
310 (16)			
299 (7)	300 (11), sh		$\nu_4(A_1)$, $\delta_s(FTeF_4)$
297 (6)			
251 (17)	252 (10)		$\nu_7(B_2)$, $\delta_{sciss}(TeF_4)$
249 (16), sh			
233 (13)	234 (16)		
225 (8)	228 (11), sh		$\nu_{11}(E)$, $\delta_{as}(TeF_4)$
212 (3)	193 (7)		
204 (3)			
189 (9)			
180 (12)			
173 (10)	177 (4)		$\delta(TeOM)$
135 (25)	126 (56)		
113 (12)	111 (35)		
100 (1)			
90 (3)	73 (49)		lattice mode or $\tau(TeOM)$

[a] The spectra were recorded on microcrystalline powders sealed in Pyrex glass melting point capillaries at room temperature using 514.5-nm excitation; values in parentheses denote relative intensities, and sh denotes a shoulder. [b] No assignments have been made for the bands in this region. Similar bands have been observed in the Raman spectra of the $M(OTeF_5)_6^-$ anions (M = As, Sb, Bi).

expected to be very weak in the Raman spectrum and therefore is not assigned. Additional splittings are observed in the Raman spectrum of $Te(OTeF_5)_4$ for the bands assigned to the $Te^{IV}F_4$ stretching frequencies $\nu_1(A_1)$ and $\nu_5(B_1)$ and for the $Te^{IV}F_4$ bending frequencies $\nu_9(E)$, $\nu_4(A_1)$, $\nu_7(B_2)$, and $\nu_{11}(E)$. The splittings are presumed to arise from axial $OTeF_5$ groups that are fluorine bridged through one of their equatorial fluorines to the central Te^{IV} atom of a neighboring $Te(OTeF_5)_4$ molecule (see **X-ray Crystal Structure of $Te(OTeF_5)_4$** and Figure 3c). The modes associated with the $Te^{IV}O_4$ moiety of $Te(OTeF_5)_4$ are treated as a XY_2Z_2 skeleton having C_{2v} point symmetry. The symmetric axial TeO_2 stretching mode is expected to exhibit a strong Raman intensity whereas the antisymmetric mode is expected to be only weakly allowed. Both the antisymmetric and symmetric equatorial $Te^{IV}O_2$ modes are expected to be Raman active. The modes associated with the $Te^{IV}O_5$ moiety of the $Te(OTeF_5)_5^-$ anion are treated as a XY_4Z C_{4v} skeleton. The symmetric XY_4 modes are expected to exhibit strong Raman intensities, whereas the antisymmetric XY_4 stretch is expected to be very weak if XY_4 is planar. However, the vibrational modes associated with the $Te^{IV}-O-Te^{VI}$ linkages of both species are expected to be strongly coupled because the oscillator components share the same central light atom and are expected to have similar frequencies, so that assignments of specific $Te^{IV}-O_{ax,eq}$ and $Te^{VI}-O_{ax,eq}$ are not possible. The general assignments were aided by comparison with the strongly coupled and intense M−O, Xe−O, and Te−O stretching modes in the $M(OTeF_5)_6^-$ anions (M = As, Sb, Bi; 392−443 cm^{-1}),[3] $Xe(OTeF_5)_2$ (428, 442 cm^{-1}),[29] $FXeOTeF_5$ (457 cm^{-1}),[41] and $XeOTeF_5^+$ (487 cm^{-1})[29] and the M−O−Te and Xe−O−Te bends of the $M(OTeF_5)_6^-$ anions (118−140 cm^{-1}),[3] $Xe(OTeF_5)_2$ (133 cm^{-1}),[29] and $XeOTeF_5^+$ (174 cm^{-1}).[29] The assignment of a Te−O−Te torsion in the $Te(OTeF_5)_5^-$ anion at 79 cm^{-1} is more tenuous and may represent a lattice mode. Moderately strong bands in the region 790−905 cm^{-1} are observed in the spectra of both $Te(OTeF_5)_4$ and the $Te(OTeF_5)_5^-$ anion and are not assigned. These bands appear to be associated with the strongly coupled $Te^{VI}-O/M-O$ stretches of the $Te^{VI}-O-M-O-Te^{VI}$ (M = Te^{IV}) linkages as similar bands have been observed in the Raman spectra of the $M(OTeF_5)_6^-$ anions (M = As, Sb, Bi)[3] and in $Xe(OTeF_5)_2$.[42] These features are absent in the spectra of the $XeOTeF_5^+$ salts,[42] $ClTeF_5$, $ClOTeF_5$, and $FOTeF_5$.[40]

The assignments for the $N(CH_3)_4^+$ cation of the $Te(OTeF_5)_5^-$ salt are based on those for the free cation, which belongs to the point group T_d and has 19 fundamental vibrations, $3A_1 + A_2 + 4E + 4T_1 + 7T_2$. Of these, the T_2 modes are infrared active and the A_1, E, and T_2 modes are Raman active. Although the assignments for the $N(CH_3)_4^+$ cations generally follow those previously given for other $N(CH_3)_4^+$ salts[3,43−48] and require little further comment, they do exhibit some interesting features which have been discussed in detail in an earlier paper related to the syntheses and characterization of the $N(CH_3)_4^+M(OTeF_5)_6^-$ (M = As, Sb, Bi) salts.[3] Our assignments of the $N(CH_3)_4^+$ cation in the previous and present work are largely based upon a previous study by Kabisch[46] of the deviations of the Raman spectra of the free $N(CH_3)_4^+$ cation from the T_d selection rules

(41) Sladky, F. *Monatsh. Chem.* **1970**, *101*, 1571.
(42) Keller, N.; Schrobilgen, G. J. *Inorg. Chem.* **1981**, *20*, 2118.
(43) Berg, R. W. *Spectrochim. Acta, Part A* **1978**, *34A*, 655.
(44) Bottger, G. L.; Geddes, A. L. *Spectrochim. Acta* **1978**, *21*, 1708.
(45) Kabisch, G.; Klose, M. J. *Raman Spectrosc.* **1978**, *7*, 312.
(46) Kabisch, G. *Raman Spectrosc.* **1980**, *9*, 279.
(47) Wilson, W. W.; Christe, K. O.; Feng, J.; Bau, R. *Can. J. Chem.* **1989**, *67*, 1898.
(48) Christe, K. O.; Wilson, W. W.; Wilson, R. D.; Bau, R.; Feng, J. *J. Am. Chem. Soc.* **1990**, *112*, 7619.

in various salts of known crystal structures, providing empirical rules for estimating, from vibrational spectra, the degree of $N(CH_3)_4^+$ cation distortion. It can be concluded that in $N(CH_3)_4^+Te(OTeF_5)_5^-$ the distortion of the $N(CH_3)_4^+$ cations from tetrahedral symmetry is also minimal. It should be noted that the Raman spectrum of $N(CH_3)_4^+Te(OTeF_5)_5^-$ presents some specific features previously reported for $N(CH_3)_4^+Bi(OTeF_5)_6^-$.[3] In particular the broadening of the $\nu_5(E)/\nu_{14}(T_2)$ bands which has been suggested to be related to short C···F contacts is indicative of weak hydrogen bonding between the methyl groups of the cation and the fluorines of the anion as indicated by the X-ray crystal structure results.

Conclusions

The gross geometries of $Te(OTeF_5)_4$ and the $FTe(OTeF_5)_4^-$ and $Te(OTeF_5)_5^-$ anions are little influenced by steric interactions among $OTeF_5$ groups. The primary bonding in $Te(OTeF_5)_4$ is consistent with an AX_4E VSEPR arrangement of Te^{IV}–O bond pair domains and a lone electron pair. Incorporation of secondary contacts with two neighboring fluorines results in a seven-coordinate AX_4Y_2E VSEPR arrangement which assumes a distorted octahedral geometry about Te^{IV}. The existence of fluorine bridges between Te^{IV} and $OTeF_5$ groups of neighboring $Te(OTeF_5)_4$ molecules in the solid state and the formation of the $Te(OTeF_5)_5^-$ anion are indicative of the moderately strong Lewis acid properties of five-coordinate Te^{IV} in $Te(OTeF_5)_4$. Both $FTe(OTeF_5)_4^-$ and $Te(OTeF_5)_5^-$ exhibit pseudo-octahedral arrangements for the lone electron pair and ligand atoms bonded to Te^{IV} and may be described in terms of AX_5E VSEPR arrangements of five bond pairs and a lone electron pair. The unique axial fluorine of the $FTe(OTeF_5)_4^-$ anion is trans to the lone electron pair. Among the square pyramidal and square planar main-group and transition metal $OTeF_5$ derivatives that are known, the $Te(OTeF_5)_5^-$ anion has afforded the first opportunity to study the effects of an axial $OTeF_5$ group on relative $OTeF_5$ group conformations in a pseudo-octahedral $OTeF_5$ derivative having an AX_5E VSEPR arrangement.

Contrasting with their isoelectronic iodine(V) mixed analogs, $F_nI(OTeF_5)_{5-n}$, which have all been characterized in IF_5 solution by ^{19}F NMR spectroscopy, and with mixtures containing only $FTe(OTeF_5)_4^-$ and $Te(OTeF_5)_5^-$, mixtures containing the more highly fluorinated anions undergo fluorine exchange among Te^{IV} sites as well as $OTeF_5$ group exchange.

Experimental Section

Apparatus and Materials. Manipulations involving volatile materials were performed under strictly anhydrous conditions on a Pyrex glass vacuum line equipped with greaseless J. Young glass/PTFE stopcocks. Nonvolatile materials were handled in the dry nitrogen atmosphere of a glovebox (Vacuum Atmospheres Model DLX).

The reagents TeO_2 (British Drug House, Analar Grade), aqueous HF (Fluka, 49% aqueous, >99% purity), *n*-Bu_4NOH (Fluka, 55–60% aqueous, >97% purity), and CH_3OH (British Drug House, 99.8%) were used without further purification. The reagents $Te(OTeF_5)_4$,[2,24] $N(CH_3)_4^+OTeF_5^-$,[3] $N(CH_2CH_3)_4^+OTeF_5^-$,[3,4] and XeF_2[49] were prepared as described previously. Literature methods were used for the purification of SO_2ClF (Aldrich and Columbia Organic Chemical),[50] Freon 114 (Aldrich),[3] and CH_2Cl_2 (Caledon).[3]

$N(n\text{-}Bu)_4^+TeF_5^-$. Only a cursory description of the synthesis of $N(n\text{-}Bu)_4^+TeF_5^-$ appears in the literature;[14] consequently a detailed description is provided here. Tellurium dioxide was weighed into a Teflon beaker. Aqueous hydrofluoric acid (49%, 30 mL) was added to the TeO_2 which dissolved upon stirring. Aqueous hydrofluoric acid (49%) was added to a solution of *n*-Bu_4NOH in CH_3OH (40%, 32.5 mL) at 0 °C in a Teflon beaker until in slight excess. The TeO_2/HF and *n*-Bu_4NOH/HF/CH_3OH solutions were combined and then evaporated in a Teflon beaker on a steam bath for 5 h giving an upper organic phase and a lower aqueous phase. Upon cooling of the mixture to room temperature and the addition of ca. 30 mL of deionized water, the organic layer rapidly crystallized as colorless needles. The mixture was stirred and then filtered through an FEP Büchner funnel. The crystals were washed three times with ca. 8 mL of 15% aqueous hydrofluoric acid and air dried on the Büchner funnel for 1 h. The crystalline product was transferred into a $^1/_2$ in. o.d. FEP tube equipped with a Kel-F valve and pumped under dynamic vacuum for 18 h to remove residual H_2O and HF. The product (5.15 g; 37% yield) was stored in an FEP vial inside the drybox until used.

$N(CH_2CH_3)_4^+Te(OTeF_5)_5^-$. The synthesis of $N(CH_2CH_3)_4^+Te(OTeF_5)_5^-$ is similar to that described for $N(CH_3)_4^+Te(OTeF_5)_5^-$ (*vide infra*), except dry CH_2Cl_2 was used as the solvent. The reactants $Te(OTeF_5)_4$ (3.2285 g, 2.984 mmol) and $N(CH_2CH_3)_4^+OTeF_5^-$ (1.1095 g, 3.008 mmol) were added to one limb of a two-limbed glass vessel containing a Teflon stir bar, and ca. 10 mL of CH_2Cl_2 was condensed onto the solids at −196 °C. The reagents dissolved upon warming to room temperature and with stirring. The solution was filtered by pouring through a medium-porosity glass frit joining the two limbs of the reaction vessel. Several aliquots of CH_2Cl_2 were condensed back into the empty limb at −196 °C to rinse it and then poured back through the frit. Finally, all the CH_2Cl_2 solvent was condensed into the empty limb and sealed off. The resulting slightly off white solid was pumped under dynamic vacuum for several hours prior to transferring to an FEP storage vessel in the drybox (yield 4.2097 g, 97.2%).

$Te(OTeF_5)_4$ and $N(CH_3)_4^+Te(OTeF_5)_5^-$. Synthesis and Crystal Growing. $Te(OTeF_5)_4$. Single crystals of $Te(OTeF_5)_4$ were grown by slow vacuum sublimation at ambient temperature in a sealed evacuated glass tube. Approximately 100 mg of $Te(OTeF_5)_4$ was loaded into a previously vacuum-dried 12-mm glass tube equipped with a glass to metal seal and connected to a Hoke 4171M2B brass bellows valve. The tube was evacuated to 10^{-6} Torr while maintaining the sample at −196 °C whereupon the sample was warmed to room temperature and pumped on for several minutes before cooling to −196 °C and heat sealing under dynamic vacuum. The tube was allowed to stand at ambient temperature for 10 months. Several colorless crystals formed on the tube walls. The tube was cut open in the drybox, and the crystals were pryed off and mounted in glass Lindemann capillaries. The crystal used in this study was a parallelepiped with dimensions 0.58 × 0.3 × 0.15 mm.

$N(CH_3)_4^+Te(OTeF_5)_5^-$. Freshly sublimed $Te(OTeF_5)_4$ (2.0353 g, 1.8811 mmol) and $N(CH_3)_4^+OTeF_5^-$ (0.5895 g, 0.1885 mmol) were loaded into separate limbs of a two-limb Pyrex vessel equipped with J. Young stopcocks in the drybox. The vessel was attached to a glass vacuum line and SO_2ClF (ca. 5 mL) distilled on to the $Te(OTeF_5)_4$ at −78 °C. On warming of the mixture to room temperature, the $Te(OTeF_5)_4$ dissolved in the SO_2ClF and the resulting solution was then poured on to the $N(CH_3)_4^+OTeF_5^-$. The empty limb was rinsed (three times) with SO_2ClF by chilling it and decanting the condensed SO_2ClF back into the limb containing the reactants in order to ensure that all the $Te(OTeF_5)_4$ had transferred. The $N(CH_3)_4^+OTeF_5^-$ rapidly dissolved giving a clear colorless solution. Freon 114 was distilled *in vacuo* into the empty limb of the vessel while keeping the stopcock between the two limbs closed. When the Freon 114 had warmed to room temperature, the interconnecting stopcock was opened, allowing the Freon 114 vapor to diffuse into the SO_2ClF solution. Clusters of large colorless platelike crystals formed over a period of 2 weeks. The supernatant liquid comprised two layers which were decanted away from the crystals. The crystals were rinsed with Freon 114 and pumped dry in dynamic vacuum before being transferred in a drybox. Some of the crystals were cut with a scalpel and mounted in 0.3, 0.4, and 0.5 mm Lindemann glass capillaries and stored at room temperature prior to mounting on the diffractometer since they proved to undergo a phase transition when kept at −78 °C. The crystals, observed under a polarizing microscope, appeared to be single or perfectly twinned. The crystal used in this study was a thick plate with dimensions 0.30 ×

(49) Mercier, H. P. A.; Sanders, J. C. P.; Schrobilgen, G. J.; Tsai, S. S. *Inorg. Chem.* **1993**, *32*, 386.
(50) Schrobilgen, G. J.; Holloway, J. H.; Granger, P.; Brevard, C. *Inorg. Chem.* **1978**, *17*, 980.

0.45 × 0.55 mm. Following X-ray data collection, the Raman spectrum of the single crystal was obtained and shown to be identical to the bulk sample.

Crystal Structure Determination of $Te(OTeF_5)_4$ and $N(CH_3)_4^+Te(OTeF_5)_5^-$. Collection and Reduction of X-ray Data. A crystal of $Te(OTeF_5)_4$ was centered on a Siemens/Syntex $P2_1$ diffractometer, using silver radiation monochromatized with a graphite crystal (λ = 0.560 86 Å). A crystal of $N(CH_3)_4^+Te(OTeF_5)_5^-$ was centered on a Siemens P4 diffractometer equipped with a rotating anode using molybdenum radiation monochromatized with a graphite crystal (λ = 0.710 73 Å). Examination of the peak profiles of $N(CH_3)_4^+Te(OTeF_5)_5^-$ revealed they were slightly broadened but single. The experimental values for the $Te(OTeF_5)_5^-$ anion, when they differ from those of the $Te(OTeF_5)_4$ compound, are given in brackets. Accurate cell dimensions were determined at T = −97 °C [24 °C] from a least-squares refinement of the setting angles (χ, ϕ, and 2θ) obtained from 26 [31] accurately centered reflections (with 15.04° [10.47°] ≤ 2θ ≤ 46.05 [25.00°]) chosen from a variety of points in reciprocal space. Integrated diffraction intensities were collected using an ω [θ−2θ] scan technique with scan rates varying from 3 [1.5] to 14.65 °/min (in 2θ) and a scan range of ±0.5 [0.54]° so that weak reflections were examined most slowly to minimize counting errors. The data were collected with $-1 \le h \le 14$ [11], -14 [-1] ≤ $k \le 14$ [21], and -15 [-1] ≤ $l \le 15$ [29] and 3 [2] ≤ $2\theta \le 50$ [45]°. During data collection, the intensities of three standard reflections were monitored every 97 [100] reflections to check for crystal stability and alignment. A total of 6079 [6658] unique reflections remained after averaging of equivalent reflections of which only 5212 [1979] satisfied the condition $I \ge 2[1.5]\sigma(I)$ and were used for structure solution. No decay was observed for $Te(OTeF_5)_4$, while some decay was observed (~10%) for $N(CH_3)_4^+Te(OTeF_5)_5^-$ and was corrected. Corrections were made for Lorentz and polarization effects. An empirical absorption correction was applied to the data of $Te(OTeF_5)_4$ by using the PSI SCAN method[51] ($\Delta\phi$ = 10°, $\mu\bar{R}$ = 0.755), while the program DIFABS[52] was used for the $Te(OTeF_5)_5^-$ anion.

Crystal Data. $O_4F_{20}Te_5$ (f_w = 1082.0) crystallizes in the triclinic system, space group $P\bar{1}$, with a = 9.502(3) Å, b = 9.748(5) Å, c = 10.603(4) Å, α = 85.73(4)°, β = 72.50(3)°, and γ = 71.26(3)°; V = 886.7(6) Å^3; D_{calc} = 4.052 g cm^{-3} for Z = 2. Ag Kα radiation (λ = 0.560 86 Å, μ(Ag Kα) = 4.40 mm^{-1}) was used. $C_4H_{12}O_5F_{25}Te_6$ (f_w = 187.0) crystallizes in the orthorhombic system, space group *Pbca*, with a = 11.021(2) Å, b = 20.096(5) Å, and c = 27.497(5) Å; V = 6090(2) Å^3; D_{calc} = 3.042 g cm^{-3} for Z = 8. Mo Kα radiation (λ = 0.710 73 Å, μ(Mo Kα) = 5.84 mm^{-1}) was used.

Solution and Refinement of the Structure. The XPREP program[53] confirmed the original cells and space groups. All calculations were performed on a 486 personal computer using the SHELXTL PLUS (Sheldrick, 1993)[53] determination package for structure solution and refinement as well as structure determination molecular graphics.

$Te(OTeF_5)_4$. The lattice was triclinic primitive (R_{int} = 0.013). The structure was shown to be centrosymmetric by an examination of the E-statistics (calc, 0.949; theor, 0.968), and consequently the structure was solved in the space group $P\bar{1}$. A first solution was obtained without absorption corrections by direct methods which located the positions of all atoms, except one fluorine, confirming the presence of the $Te(OTeF_5)_4$ compound. The full matrix least-squares refinement of the Te, O, and F atoms gave a conventional agreement index R_1 of 0.0957. A difference Fourier synthesis revealed the last fluorine atom. Refinement of positional and isotropic temperature parameters for all atoms converged at R_1 = 0.0689.

The structure was solved a second time using data that had been corrected for absorption. All atoms could be refined anisotropically. The final refinement was obtained by setting the weight factor to $1/[\sigma^2(F_o^2) + (0.0737P)^2 + 0.0P]$ and gave rise to a residual, R_1, of 0.0239 (wR_2 = 0.0577). In the final difference map, the maximum and the minimum electron densities were 1.12 and −0.86 e Å^{-3}.

$N(CH_3)_4^+Te(OTeF_5)_5^-$. The lattice was orthorhombic primitive (R-int = 0.042). The only space group which was consistent with the systematic absences was the centrosymmetric *Pbca* space group. The structure was shown to be centrosymmetric by an examination of the E-statistics (calc., 0.934, theor., 0.968), and consequently the structure was solved in this space group. A first solution was obtained without absorption corrections, and it was achieved by direct methods which located the positions of the tellurium atoms on general positions. The full-matrix least-squares refinement of the tellurium atom positions and isotropic thermal parameters, the weight factor being set equal to zero, gave a conventional agreement index R_1 of 0.212. The following difference Fourier synthesis clearly revealed the five bridging oxygen atoms as well as the five fluorines of the axial $OTeF_5$ group, all of them being on general positions (R_1 = 0.196), and confirmed the square pyramidal geometry of the anion. All of the remaining fluorine atoms and the nitrogen and carbon atoms of the cation were located on general positions by successive difference Fourier syntheses. Refinement of positional and isotropic temperature parameters revealed large thermal parameters, especially for the fluorine atoms associated with the equatorial $OTeF_5$ groups. The anisotropies of the carbon atoms were also high.

The structure was solved a second time using data that had been corrected empirically for absorption. The final refinement was obtained by introducing a weight factor ($w = 1/\sigma^2(F) + 0.000171F^2$), and all the O atoms and one of the fluorine atoms (F(15)) were kept isotropic and gave rise to a residual, R_1, of 0.1044 (R_w = 0.0781). In the final difference Fourier map, the maximum and the minimum electron densities were +1.48 and −1.09 e Å^3.

The final value of 0.1044 for the residual, R, is not as low as might be desired and likely arises from our inability to adequately compensate for absorption. This is reflected by our inability to refine one of the fluorine atoms anisotropically. In addition, the authors were unable to work at low temperature owing to a phase transition (ca. 0 to −30 °C), and the crystal diffracted weakly and only at low angles (only 30% of the reflections were used in the refinement). However, the uncertainties on the variables that were refined are comparable to those observed in $U(OTeF_5)_6$.[36]

Nuclear Magnetic Resonance Spectroscopy. All spectra were recorded unlocked (field drift <0.1 Hz h^{-1}) on a Bruker AM-500 spectrometer equipped with an 11.744-T cryomagnet and an Aspect 3000 computer. The ^{19}F spectra were obtained using a 5-mm combination $^1H/^{19}F$ probe operating at 470.599 MHz. The spectra were recorded in a 32 K memory. A spectral width setting of 20 or 50 kHz was employed, yielding data point resolutions of 1.2 and 30 Hz/data point and acquisition times of 0.82 and 0.33 s, respectively. No relaxation delays were applied. Typically, 750−4000 transients were accumulated. The pulse width corresponding to a bulk magnetization tip angle, θ, of approximately 90° was equal to 1 μs. No line-broadening parameters were used in the exponential multiplication of the free induction decays prior to Fourier transformation.

The ^{125}Te spectra were obtained using a 10-mm broad-band VSP probe (tunable over the range 23−202 MHz) which was tuned to 157.794 MHz to observe ^{125}Te. Free induction decays for ^{125}Te were accumulated in 16 K memories with spectral width settings of 30 or 50 kHz and yielded acquisition times of 0.28 and 0.16 s and data point resolutions of 3.6 and 6.1 Hz/data point, respectively. No relaxation delays were applied. Typically, 10 000−45 000 transients were accumulated for the ^{125}Te spectra. The pulse width corresponding to a bulk magnetization tip angle, θ, of approximately 90° was 18 μs. Line-broadening parameters used in the exponential multiplication of the free induction decays were 3−7 Hz.

The ^{19}F and ^{125}Te NMR spectra were referenced to external samples of neat $CFCl_3$ and $Te(CH_3)_2$, respectively, at 30 °C. The chemical shift convention used is that a positive (negative) sign indicates a chemical shift to high (low) frequency of the reference compound.

The ^{19}F and ^{125}Te NMR samples were prepared in 5-mm medium-wall and in 10-mm o.d. thin-wall precision glass NMR tubes (Wilmad), respectively. Samples of recrystallized $N(CH_3)_4^+Te(OTeF_5)_5^-$ were weighed into the previously dried NMR tubes in the drybox. The tubes were closed with Kel-F valves and transferred to a glass vacuum line, and SO_2ClF or CH_2Cl_2 solvent was distilled *in vacuo* on to the solid at

(51) North, A. C. T.; Phillips, D. C.; Mathews, F. S. *Acta Crystallogr.* **1968**, *A24*, 351.
(52) Walker, N; Stuart, D. *Acta Crystallogr.* **1983**, *A39*, 158.
(53) Sheldrick, G. M. SHELXTL PLUS Release 4.21/V. Siemens Analytical X-Ray Instruments. Inc., Madison, WI, 1993.

−78 °C. The tubes were heat-sealed in dynamic vacuum while keeping the contents frozen to −196 °C.

Raman Spectroscopy. Raman spectra were recorded on a Jobin-Yvon Mole S-3000 spectrograph system equipped with a 0.32-m prefilter, adjustable 25-mm entrance slit, and a 1.00-m triple monochromator. Holographic gratings were used for the prefilter (600 grooves mm^{-1}, blazed at 500 nm) and monochromator [1800 grooves mm^{-1} ($N(CH_3)_4^+Te(OTeF_5)_5^-$) or 2400 grooves mm^{-1} ($Te(OTeF_5)_4$) both blazed at 550 nm] stages. An Olympus metallurgical microscope (Model BHSM-L-2) was used for focusing the excitation laser to a 1-μm spot on the sample. The 514.5-nm line of an Ar ion laser was used for excitation of the sample. Spectra were recorded at ambient temperature on a powdered microcrystalline samples sealed in a baked-out Pyrex melting point capillaries as well as on the single crystals used to determine the X-ray structures sealed in their original glass Lindemann capillaries. The spectra were recorded by signal averaging using a Spectraview-2D CCD detector equipped with a 25-mm chip (1152 × 298 pixels) and at a laser power of 20 mw at the sample and slit settings corresponding to a resolution of 1 cm^{-1}. A total of 10 reads having 30 s integration times were summed. Spectral line positions are estimated to be accurate to ±1 cm^{-1}.

Acknowledgment. We thank Prof. K. O. Christe for his helpful comments and suggestions relating to the manuscript and the donors of the Petroleum Research Fund, administered by the American Chemical Society, for support of this work under ACS-PRF No. 26192-AC3.

Supporting Information Available: A structure determination summary (Table 6), anisotropic thermal parameters (Table 7), and atomic coordinates for the hydrogen atoms (Table 8) for $N(CH_3)_4^+Te(OTeF_5)_5^-$ and $Te(OTeF_5)_4$, ^{19}F and ^{125}Te NMR spectra of TeF_5^- (Figure 7), a unit cell of $Te(OTeF_5)_4$ (Figure 8), and a stereoview ORTEP of the packing in the unit cell (Figure 9) (11 pages). Ordering information is given on any current masthead page.

IC9402665